Memoirs of the School of Engineering, Nagoya University
Vol.51, No.1 (1999)

# PROCESS ANALYSES FOR DEVELOPING COST-EFFECTIVE PARTICULATE REINFORCED INORGANIC COMPOSITES

Takao CHOH

*Department of Materials Processing Engineering*

(Received May 18, 1999)

**Abstract**

The mechanical properties of composites are extremely controlled by the structure and properties of the reinforcement / matrix interface. These controlling factors are affected by fabrication process including operation time and temperature and the kind of matrix or reinforcement. In this paper, for developing cost-effective particulate reinforced inorganic matrix composites, some fabrication processes were proposed. From this point of view, the incorporation process and the wettability for ceramic / aluminum systems were evaluated by the time required for the incorporation of the ceramic particles into the molten aluminum during melt stirring. The effects of alloying element on the incorporation time and properties of composite were also measured. As a new fabrication process, stable carbide particles such as TiC were *in situ* synthesized in the liquid aluminum by reaction between the Al-Ti alloy and SiC or $Al_4C_3$ particles. Reactive infiltration of solid powder blends with molten aluminum or magnesium has been investigated as a potential route for the synthesis of a particulate reinforced metal matrix composite as well as an $Al_2O_3$ matrix composite.

**Keywords:** composite, wettability, melt stirring method, particle dispersion, reactive infiltration, *in situ* reaction, exothermic reaction, molten metal, ceramic powder

**Contents**

## Introduction

A great deal of effort has been made to the development of the metal matrix composite (MMC) that offers advantages in the application concerning low density, high strength and high stiffness. However, the industrial application of MMC has been disturbed by extreme high production costs and complex processes. In this view-point, a particle-reinforced metal matrix composite has advantages in the ease of fabrication, low cost and absence of anisotropy of mechanical properties. So, this paper will mainly focus on the fabrication process of the particle-reinforced inorganic composites, for increase in the commercial application of the composites, considering interfacial phenomena, which include reactions between the metals and ceramics, wettability of the ceramic with the molten metal and *in situ* synthesis of the ceramics.

## 1 Incorporation Behavior of Ceramic Particles into the Molten Aluminum by Melt Stirring Process

### 1.1 Introduction

In general, MMC are classified in three types by the configurations of the reinforcements such as particulate-reinforced metal composite, whisker-reinforced metal composite and fiber-reinforced metal composite. These composites are fabricated mainly by powder metallurgy, compocasting, squeeze casting and melt-stirring method. In these composites, particulate-reinforced metal matrix composite can be manufactured easier by the melt-stirring method. However, this method has some problems about the uniformity of particulate distribution and the amount of incorporated particles in the melt. These problems almost depend on the wettability between the

molten metal and the ceramic particle. The wettability has often been measured by the sessile drop method and quantitatively estimated by using the contact angle, $\theta$. However, the wettability for a system of solid particle / liquid metal cannot simply be estimated by the contact angle, because of small radius of the particle. Then, Oh *et al*[1] reported the wettability between the carbide particle and liquid metals by using a pressure infiltration method. In the present work, the wettability between the ceramic particle and aluminum alloy has been evaluated from the time necessary for particulate incorporation into the liquid aluminum during the melt stirring, and then the incorporation processes of SiC, ZrC and AlN particles into the molten aluminum and its alloy were analyzed. Furthermore, the interfacial phenomena between these particles incorporated and aluminum matrix were discussed[2)-5)].

## 1.2 Experimental procedure

In this experiment, SiC (3.14 and 20 $\mu$m), ZrC (2.4 $\mu$m) and AlN (6.32 $\mu$m) were used as particulate reinforcement. Component of experimental materials are given as follows; Al: pure metal (99.75 mass % Al), Mg: pure metal (99.9 mass % Mg), Zn: Pure metal (99.9 mass % Zn), Si: Al-24.3 mass % Si alloy, Sn: pure metal (99.95 mass % Sn), Ti: Al-5.01 mass % Ti alloy, Cu: pure metal (99.99 mass % Cu), Pb: pure metal (99.9 mass % Pb), Bi: pure metal (99.9 mass % Bi), Li: Al-18.5 mass % Li alloy.

The volume fraction of these particles in the composite was 12 % and 17.7 % for SiC, 12 % for ZrC and 10 % for AlN. A total amount of 60 g of aluminum or aluminum alloy was melted in a magnesia crucible (inner diameter 38 mm) under an argon atmosphere in an induction furnace shown in Fig. 1-1[4]. During melt was held at a experimental temperature of 1023 K for SiC and ZrC or 1273 and 1473 K for AlN , these particles wrapped in an aluminum foil were preheated above the melt for 600 s. Then particles were added to the liquid aluminum and melt stirring was started by using an alumina rod. Melt stirring was continued for a certain period after the particulate incorporation had finished to improve the uniformity of particulate distribution. The fabri-

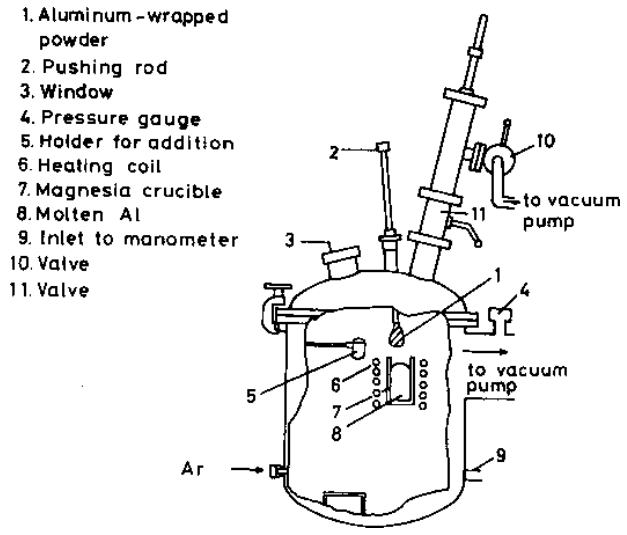


Fig. 1-1 Schematic view of induction furnace.

cated composite was poured into a metallic mold. When viscosity of the melt was too high to cast, composite was cooled in the crucible. The obtained ingot was hot extruded at a temperature of 773 K. The specimens were then sectioned and examined by electron probe microanalysis (EPMA) and scanning electron microscopy (SEM). Some of the test pieces were held at 803 K for 50 and 100 h to investigate the degradation of mechanical properties at elevated temperatures.

## 1.3 Results and discussion

### 1.3.1 *Dispersion of SiC and ZrC in the molten aluminum*

(1) *Incorporation behavior of SiC particles and definition of incorporation time*

During the melt-stirring process, particles added to the melt were distinguished into incorporated particles and still unincorporated particles[2]. However, further observation enabled unincorporated SiC particles to be classified into two groups: as-powder particles and agglomerates of particles bound by aluminum. Thus the particles were classified into three groups in all: (a) as-powder particles, (b) agglomerate of particles and (c) incorporated particles. In order to measure the ratio of these three types of particulate forms, as-powder particles and agglomerates were divided by a 200 mesh screen, and incorporated particles were extracted by dissolving the aluminum matrix with NaOH aqua solution. For the SiC / pure aluminum system, the change in the ratio of these types of particle with stirring time is shown in Fig. 1-2, indicating that the ratio of as-powder SiC decreased linearly with stirring time, while the ratio of SiC particles in the agglomerate increased and then reached a maximum value at the same time as particulate incorporation started. Therefore, it is clear that SiC particles were not incorporated into the liquid aluminum immediately and an incubation time existed until SiC particles began to be incorporated into the liquid aluminum. This indicates that the SiC particles were gradually wetted by liquid aluminum, and the agglomerates were formed out of partly wetted particles. Thus the incorporation time represents a duration which is necessary for full particulate wetting. The incorporation process of SiC particles for the SiC / Al-0.5%Mg alloy system was almost the same as that of the SiC / aluminum system,

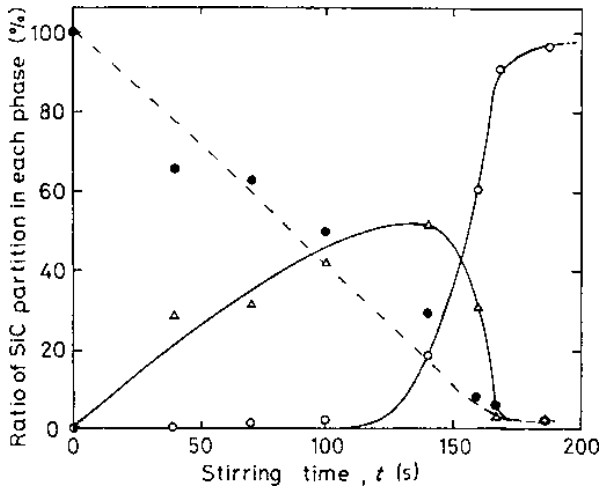


Fig. 1-2 Incorporation process of SiC particles into liquid aluminum at 1023 K: ( ● ) SiC in powder phase, ( △ ) SiC in agglomerate and ( ○ ) SiC dispersed in melt.

although the incorporation time and the incubation time were shortened. Furthermore, the incorporation process was not affected by the melt temperature, either.

A typical relation between the ratio of the incorporated particles, temperature of the liquid aluminum and the stirring time is shown in Fig. 1-3[3]. According to Fig. 1-3, particles were incorporated into the melt abruptly after a constant period or an incubation time. On the other hand, during melt stirring, an increase in the liquid temperature could be detected. This heat generation may be due to the interfacial reaction and the change in the interfacial energy ($\sigma_{sv} - \sigma_{sl}$) during the wetting process. So the incorporation time could be easily identified from the graph of stirring

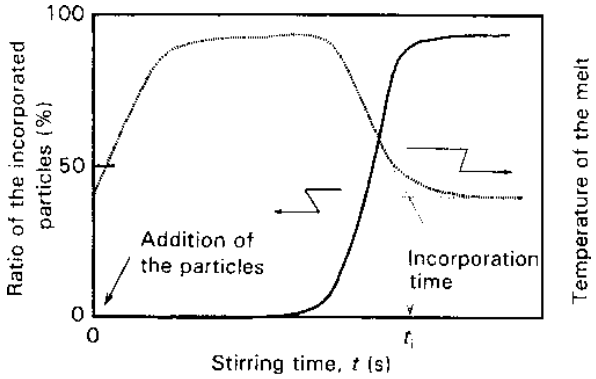


Fig. 1-3 Typical relation between the ratio of incorporated particles, temperature of the liquid phase and the stirring time.

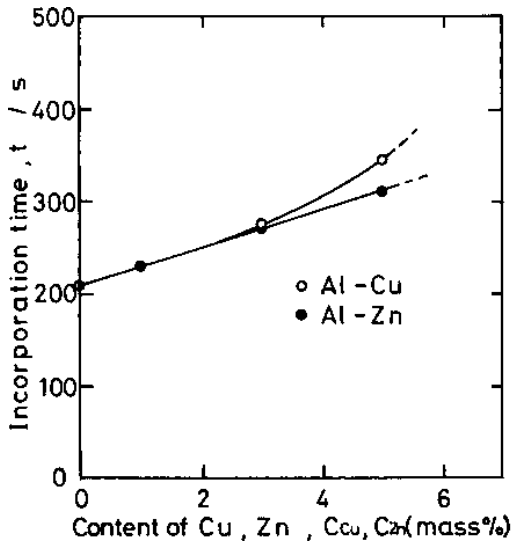


Fig. 1-4 Effects of zinc and copper on the incorporation time of SiC particles in liquid aluminum at 1023 K.

time versus temperature of the liquid phase as shown in Fig. 1-3. Hence, the wettability of ceramic particles was also estimated by this incorporation time and, in this work, the shorter incorporation time indicates the better wettability.

(2) *Effects of alloying elements on incorporation time of SiC and ZrC*

From previous work[6], it is clear that a dominant factor of wetting seems to be the dissociation of SiC given by SiC → Si + C, where Si and C denote silicon and carbon dissolved in the melt. This dissociation is promoted by the increase in solubility of Si or C and by consumption of these elements according to the reaction with alloying elements by Si + mMe = $Me_mSi$ or C + nMe = $Me_nC$. Owing to these, interfacial reaction through the dissociation of SiC particle may provide a good wettability, resulting in shortening the incorporation time.

It is clear from Fig. 1-4 that the incorporation time of SiC particles into the molten aluminum is prolonged with increase in copper or zinc addition, because these elements do not show surface active and not form their silicide or carbide by reacting with SiC for improving wettability[4].

The effect of silicon on the incorporation time of SiC and ZrC was shown in Fig. 1-5, indicating that the incorporation time of SiC was prolonged by silicon alloying, whereas that of ZrC was shortened[3]. This suggests that the wettability of ZrC was improved, and that of SiC was not. An analysis by EPMA revealed the formation of zirconium silicide in the matrix of the ZrC / Al-Si composite. Note that, as shown in Fig. 1-6, the incorporation time of SiC was shortened, and that of ZrC was prolonged by zirconium alloying. Zirconium silicide was also observed in the matrix of the SiC / Al-Zr alloy system. In these systems, good wettability can be achieved by the dissociation of ZrC : ZrC → Zr + C. Consequently, the incorporation times of SiC and ZrC were shortened by alloying zirconium for SiC and alloying silicon for ZrC, because the dissociations of ZrC and SiC seem to be enhanced by the following reaction: mZr + nSi → $Zr_mSi_n$.

In general, wettability is improved by a decrease in the surface energy of liquid surface, $\gamma_{lv}$. So, it is interesting to know the effect of a surface active element on the incorporation time. Then,

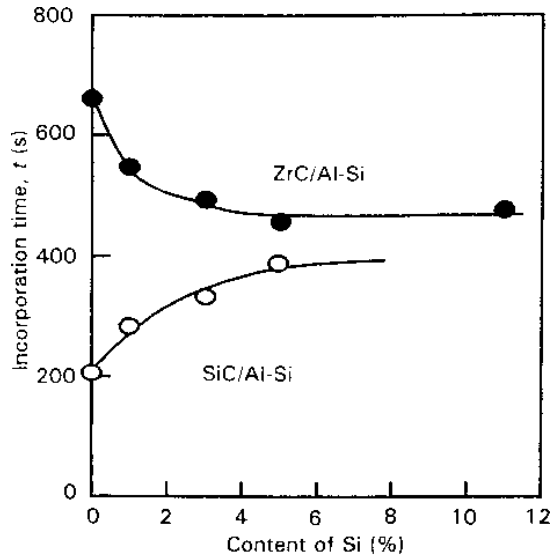


Fig. 1-5 Effect of silicon on the incorporation time of SiC (20 μm) and ZrC (2.4 μm) particles into liquid aluminum at 1023 K.

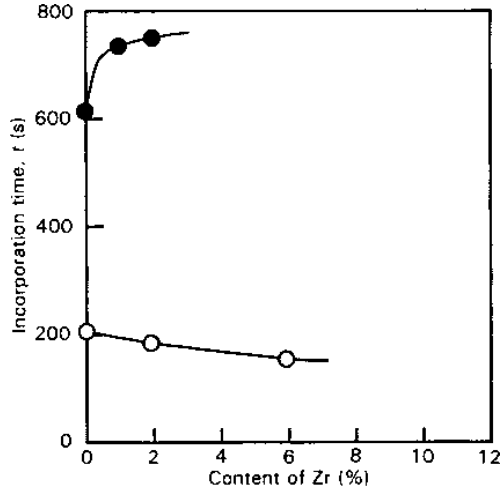


Fig. 1-6 Effect of zirconium on the incorporation time of SiC (20 μm) and ZrC (2.4 μm) particles into liquid aluminum at 1023 K: ( ● ) ZrC / Al-Zr and ( ○ ) SiC / Al-Zr.

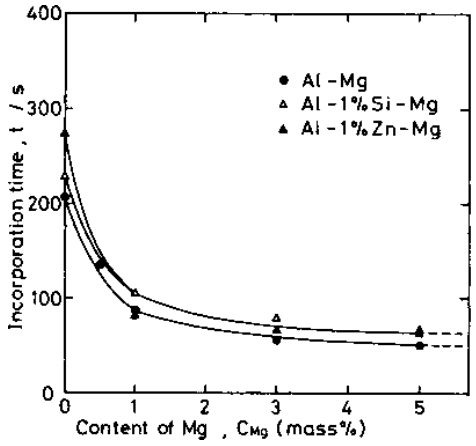


Fig. 1-7 Effects of magnesium on the incorporation time of SiC (20 μm) particles into liquid aluminum and aluminum alloys at 1023 K.

such elements as magnesium, lithium, lead, bismuth and tin which reduces the surface energy of liquid aluminum[7], were alloyed in the melt.

First of all, the effect of magnesium on the incorporation time of SiC particle was measured[3]. It is clear that incorporation time of SiC particles was shortened by magnesium alloyed in the pure aluminum and the binary alloys of Al-Si(1 %) and Al-Zn(1 %) as shown in Fig. 1-7. It is also apparent from Fig. 1-8 that the incorporation time is shortened by alloying lithium.

However, contrary to the expectation, it was extremely prolonged by alloying lead or bismuth even at low content[4]. According to Figs. 1-7 and 1-8, it is clear that lead, bismuth, magnesium and

lithium show two opposite effects on the incorporation time.

To clear this difference, surface excess concentration (Γ) was calculated with the help of the surface tension measured by Lang[7] and Gibbs' adsorption equation: $\Gamma = (-1/RT)(d\,\gamma_{lv} / d \ln a_j)$, where $a_j$ is the activity of j component, R is the gas constant, T is the temperature (K). The value of Γ of lithium could not be calculated because of the lack of the value of lithium activity in aluminum. Fig. 1-9 shows the calculated results of Γ for bismuth, lead, tin and magnesium. It is apparent that the surface excess concentrations of bismuth and lead are extremely high even at a small amount of addition less than 0.3 %. For example, only by 0.3 % addition of lead, the surface excess concentration is near to a value of the atomic density of lead's (100) plane shown by the broken line in Fig. 1-9. Thus, the surface of the aluminum melt is widely adsorbed by lead atoms.

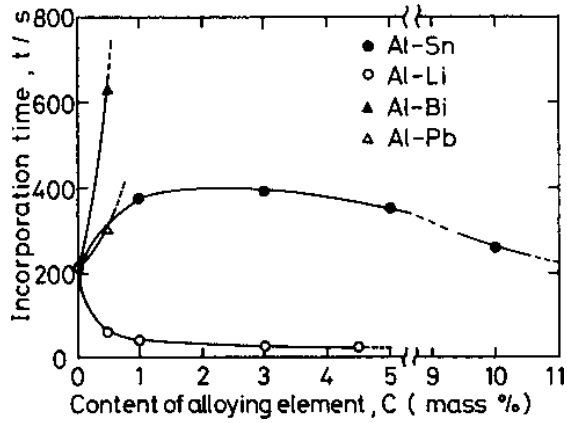


Fig. 1-8 Effects of lead, bismuth, lithium and tin on the incorporation time of SiC particles in liquid aluminum at 1023 K.

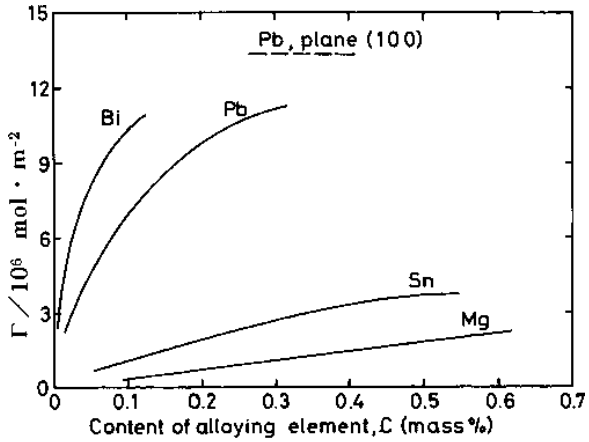


Fig. 1-9 Surface excess concentration of magnesium, tin, lead and bismuth in liquid aluminum, calculated using the data by G. Lang[7] at 1023 K.

And it is expected that other surface-active elements show a similar behavior. Furthermore, these alloying elements are considered to adsorb at the interface between the SiC particle and the melt as well as on the melt surface. Therefore, the affinity of these surface-active elements for SiC particle is more important factor than a degree of surface activity, for improving wettability by decrease in the interfacial energy between the SiC particle and the melt through joining and subsequent reaction. That is to say, although lead and bismuth atoms gather at the interface between SiC and melt, they rather behave as an obstacle to the reaction of the melt with SiC, owing to their weak affinities for SiC. Namely the extreme increase in the incorporation time is reasonably attributed to the adsorption of lead or bismuth at the interface. On the contrary, lithium and magnesium gather at the interface, subsequently join with SiC due to their strong affinities for SiC and form inter-metallic compounds such as $Mg_2Si$ and Al-Si-Li system as detected by EPMA and AES, resulting in shortening the incorporation time. As concerns SiC / Al-Sn system, the incorporation time was prolonged until tin addition was about 3 %, and after once reached at a maximum, it was shortened with increasing in tin concentration (Fig. 1-8). The reason for this change in the effect of tin still remains uncertain.

(3) *Reaction between the particle and matrix at elevated temperature*

One of the advantages required for composites is high strength at elevated temperatures. However, if interfacial reaction in the MMC occurs in an elevated-temperature, the composite's strength will be degraded. So we measured the strength and observed the microstructure of a SiC / Al alloy and a ZrC / Al alloy composites which were held at an elevated temperature[3)].

The tensile strengths of SiC / Al and ZrC / Al composites and those of composites held at elevated temperature are shown in Fig. 1-10. The testing temperature (803 K) was settled under the eutectic temperature of aluminum and silicon to prevent formation of a liquid phase. The strength of the SiC / Al composite decreased with holding time at 803 K, whereas that of the ZrC / Al composite did not. By SEM observation, the formation of reaction products could be seen in the SiC / Al composites with holding at elevated temperature. According to the X-ray microanalysis, these reaction products were confirmed as being Si and $Al_4C_3$. Furthermore, the strength of the SiC / Al-3 % Mg composite decreased rapidly with elevated-temperature holding time, as shown

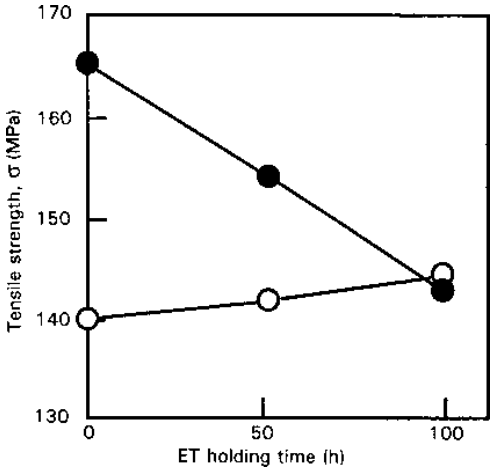


Fig. 1-10 Changes in the strength of ( ● ) SiC (20 μm) / Al and ( ○ ) ZrC (2.4 μm) / Al composite with the elevated-temperature holding at 803 K.

in Fig. 1-11. SEM observation revealed that most of the SiC particles were decomposed by forming $Mg_2Si$ during the elevated-temperature holding. On the contrary, for the ZrC / Al-3 mass % Mg composite, the strength did not decrease rapidly in comparison with the SiC / Al-3 % Mg composite because of the stability of ZrC. On the other hand, a decrease in the strength of the SiC / Al-1 % Ti composite caused by the elevated-temperature holding was much less than that for the SiC / Al-Mg composite, and it was almost equal to that of the SiC / Al composite as shown in Fig. 1-12. In this case, TiC was formed during the fabrication process and it became a diffusion barrier to titanium, silicon and carbon. Titanium alloying, therefore, not only made this system wettable,

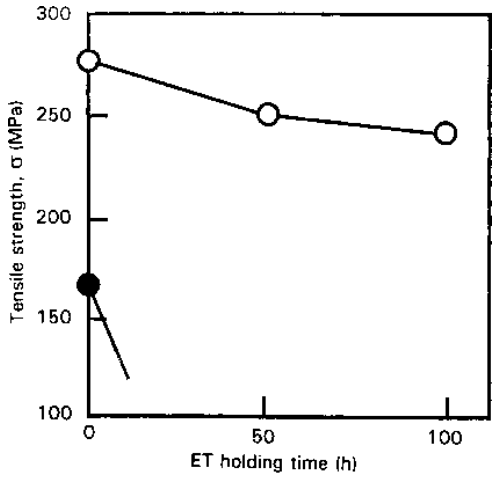


Fig. 1-11 Changes in the strength of ( ● ) SiC (3 μm) / Al-3 wt % Mg and ( ) ZrC (2.4 μm) / Al-3 wt % Mg composite with the elevated-temperature holding at 803 K.

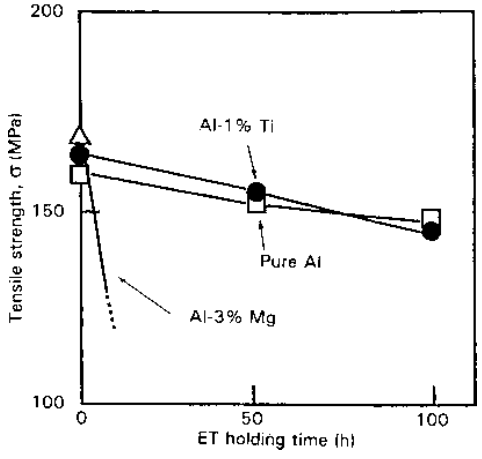


Fig. 1-12 Changes in the strength of SiC (3 μm) / Al alloy composite with the elevated-temperature holding at 803 K.

but played another role by preventing the excessive reactions as well.

### 1.3.2 *Dispersion of AlN particles in the molten aluminum*

(1) *Effects of alloying elements*

The incorporation time of the AlN / pure Al composite was the longest[5]. Furthermore, the distribution of AlN particles in the matrix was not uniform. These results can be explained by poor wettability of AlN particles with the aluminum melt as Fujii et al.[8] reported 128 deg as a contact angle between them at 1373 K. The selection of lithium and magnesium as the alloying element resulted in decreasing the incorporation time, because these elements in the melt improved the wettability. On the contrary, the addition of bismuth to the Al-Mg melt increased the incorporation time owing to the same reason as previously mentioned. Namely, bismuth acts as an obstacle to the reaction between the melt and the AlN particles due to the bismuth's lower affinity for AlN, although bismuth atoms seem to be considerably adsorbed at this interface.

It was also found that, under a nitrogen atmosphere instead of argon, the incorporation time increased. This can be explained by taking following reactions; (a) $N_2 = 2\underline{N}$ and (b) $AlN = Al + \underline{N}$, where $\underline{N}$ is the nitrogen dissolved in the melt. If the processing of an AlN / Al composite is conducted under a nitrogen atmosphere, reaction (a) will proceed from left to right. Under this condition, since the dissolved nitrogen becomes an alloying element, the dissociation of the AlN by reaction (b) for improving wettability will be hindered, resulting in prolonging incorporation time. Similar phenomena were found in both incorporation processes of SiC particles into the Al-Si alloy melt and ZrC particles into the Al-Zr as previously mentioned.

(2) *Properties of AlN particulate-reinforced aluminum composite*

The mechanical properties were measured for composites containing 10 % AlN particles fabricated under a nitrogen atmosphere[5]. An AlN / pure Al composite fabricated by stirring for 660 s at 1473 K had a minimum ultimate tensile strength such as 57 MPa, because of the presence of large agglomerates in the composite. On the other hand, the strength of an AlN / Al-Mg composite processed by stirring for 1200 s at 1273 K reached 199 MPa. This might be due to the enough joining between the AlN particles and matrix caused by a good wetting and due to the increase in the matrix strength by adding magnesium. However, fabricating by stirring for 1200 s at 1473 K, the strength of an AlN / Al-Mg composite decreased to 101 MPa, probably because of the evaporation of magnesium from the melt.

## 1.4 Conclusions

A melt stirring method was used to fabricate pure aluminum and aluminum alloys reinforced with SiC, ZrC and AlN particles. The main results of the investigations are as follows.

(1) During the particulate incorporation process, the agglomerates of SiC particles were formed until particulate incorporation began.

(2) The incorporation time was identified from the stirring time-melt temperature chart.

(3) The incorporation time of SiC was prolonged by alloying zinc, copper, bismuth and lead which have weak affinity for SiC, although bismuth and lead reduce the surface energy of the molten aluminum.

(4) The incorporation time of SiC was shortened by alloying magnesium and lithium. The reaction products of $Mg_2Si$ and Al-Si-Li system were detected by EPMA in the cases of SiC / Al-Mg and SiC / Al-Li systems, respectively.

(5) The incorporation time of SiC, ZrC or AlN particles was increased by respectively adding silicon, zirconium or nitrogen, probably because of retardation of the dissociation of these particles.

(6) The strength of the SiC / Al composite was decreased by the elevated-temperature holding

at 803 K for 50 and 100 h, although the strength of the ZrC / Al composite was not decreased.

(7) The strength of the SiC / Al-Mg composite decreased rapidly with the elevated-temperature holding due to considerable reaction of the SiC particles.

(8) In the system SiC / Al-Ti, TiC formed at the interface became diffusion barrier preventing the reaction of SiC during the elevating-temperature holding.

(9) The magnesium alloyed in the aluminum increased the strength of the composites reinforced with AlN particles, due to improving wettability and due to increasing strength of the matrix.

## References

1) S-Y. Oh, J. A. Cornie and K. C. Russell: Ceram. Eng. Sci., 8 (1987), 912.
2) M. Kobashi and T. Choh: J. Mater. Sci., 28 (1993), 684.
3) M. Kobashi, T. Mohri and T. Choh: J. Mater. Sci., 28 (1993), 5707.
4) M. Kobashi and T. Choh: Mater Trans. JIM, 31 (1990), 1101.
5) E. Taheri-Nassaj, M. Kobashi and T. Choh: Scrip. Met. Mat., 32 (1995), 1923.
6) T. Choh and T. Oki: Mater. Sci. Tech., 3 (1987), 378.
7) G. Lang: Aluminium, 51 (1974), 731, 49 (1973), 231.
8) H. Fujii, H. Nakae and K. Okada: Metall. Trans., 24A (1993), 1391.

## 2. *In Situ* Aluminum Composite Fabricated by Reaction between $Al_4C_3$ or SiC Particles and Al-Ti Alloy

### 2.1 Introduction

In the *in situ* fabrication process, the reaction between raw materials is utilized to synthesize reinforcements in the matrix. Thus the *in situ*-formed composites reveal not only excellent dispersion of fine reinforcing particles, but also high thermodynamical stability. Sahoo and Koczak[1)] already fabricated the *in situ*-formed TiC / Al composites by bubbling carbonaceous gas into the Al-Ti alloy melt. However, the process using carbonaceous gas has some practical difficulties and problems in controlling the volume fraction of the TiC particle formed. Therefore, a simplified *in situ* process is sought in order to solve these problems. The present work investigated the fabrication of *in situ*-formed TiC particulate-reinforced aluminum composites by utilizing the reaction between the Al-Ti alloy and a relatively unstable carbide such as SiC and $Al_4C_3$ as the solid carbon source instead of carbonaceous gas, to improve control of the *in situ* reaction rate and the volume fraction of carbide formed[2)].

### 2.2 Experimental procedure

In this study, aluminum ingot (99.99 % Al), titanium particles (99.7 %, under 44 μm), SiC particle (0.6, 3 and 30 μm) and $Al_4C_3$ particles (3, 14 and 30 μm) were used. In the first method, 80 g of aluminum containing titanium was melted in an induction furnace in a MgO crucible under an argon atmosphere, and held at 1473 K. Then SiC or $Al_4C_3$ particles were added and incorporated by the melt-stirring method[3)]. During this stirring, TiC particles were formed *in situ* in the melt and then the sample was cast into a mold. In the second method, the (Ti + $Al_4C_3$) powder blend was intermittently added to pure aluminum at the rate of about 1 g / 30 s at 1473 K during stirring. After incorporation of all of the $Al_4C_3$ particles, the melt temperature was lowered to 973 K and

copper was alloyed to produce the Al-5 mass % Cu matrix. Subsequently, samples were solidified and extruded at 773 K. Then, the mechanical properties were measured and the microstructure was observed by SEM. Besides, SiC (14 μm) / Al-Si and TiC (1 μm) / Al-Si composites were also fabricated by the melt-stirring method at 1073 K to compare mechanical properties with that of the *in situ* composites. The theoretical volume fraction of *in situ*-formed particles reaches 5.5 % in the first method, and 5 and 10 % in the second method, assuming complete *in situ* reaction.

### 2.3 Results and discussion

The microstructures of *in situ* composites fabricated from several sizes of SiC particles by stirring for 900 s at 1473 K are compared in Fig. 2-1. *In situ* formation of TiC particles could be confirmed by XRD and EPMA for the composite shown in Fig. 2-1(a). It is obvious from Fig. 2-1(a) that approximately 1 μm or less particles are almost uniformly dispersed in the composites fabricated by adding 0.6 μm SiC. The same distribution of *in situ*-formed particles can be achieved when adding 3 μm SiC, as shown in Fig. 2-1(b). However, using 14 μm SiC particle, as shown in Fig. 2-1(c), the circular TiC phase surrounding remaining raw SiC particles is observed as well as the large inter-metallic compounds of $Al_3Ti$ formed from the remaining titanium due to the decrease in the *in situ* reaction rate. Hence, the size of the SiC particle has an effect not only on the rate of the *in situ* reaction, but also on the dispersion behavior of *in situ*-formed TiC particles. Therefore, the ultimate tensile strength, the 0.2 % proof stress and uniform elongation of those composites were decreased with increasing diameter of SiC as shown in Fig. 2-2.

The mechanical properties of *in situ*-formed TiC / Al-5 mass % Si composite were compared with that of the composites reinforced with nearly 14 μm SiC and nearly 1μm TiC particles fabricated by the melt-stirring method as shown in Fig. 2-3. It was found that the ultimate tensile strength and 0.2 % proof stress of *in situ* TiC / Al-5 mass % Si composite were higher than those of two others fabricated by the melt-stirring method, although its uniform elongation was the lowest; i. e. strength efficiency is improved through the *in situ* reaction.

*In situ*-formed TiC / Al-5 mass % Cu composites were fabricated by the second method, where a powder blend of 3 μm $Al_4C_3$ and titanium was added to the melt. The ultimate tensile strength of the *in situ* TiC / Al-4.5 mass % Cu composite aged for 86.4 ks at 450 K after the solution heat treatment reached 530 MPa at Vf = 5.5 %, as shown in Fig. 2-4. Moreover, the strength obtained in

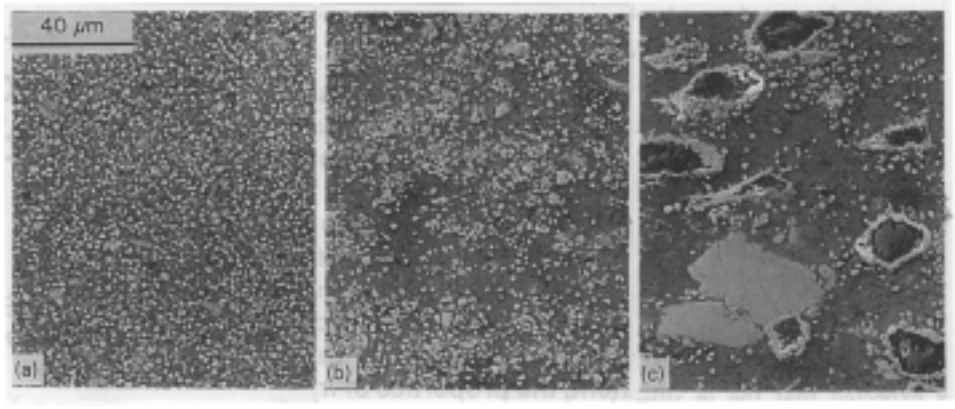


Fig. 2-1 Scanning electron micrographs of *in situ* TiC / Al composites fabricated by reaction time of 900 s at 1473 K from (a) 0.6 μm, (b) 3 μm and (c) 14 μm SiC.

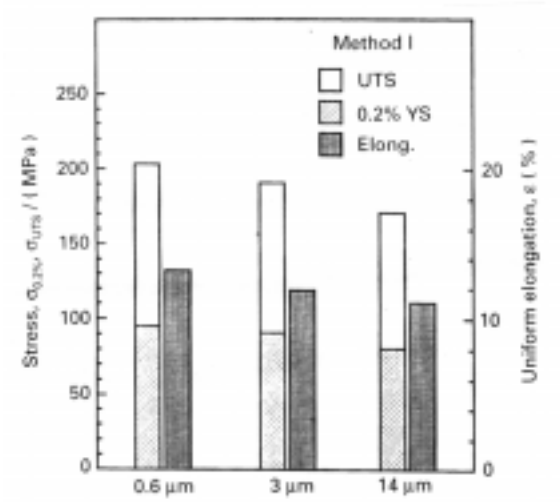


Fig. 2-2 Mechanical properties of *in situ* TiC / Al composites fabricated by reaction time of 900 s at 1473 K from (a) 0.6 μm, (b) 3 μm and (c) 14 μm SiC.

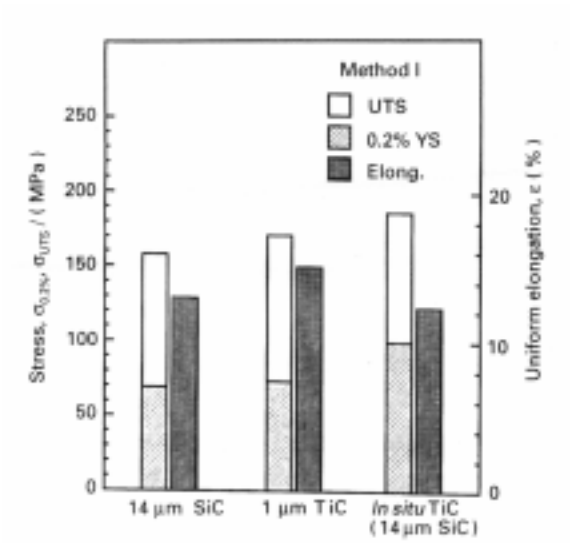


Fig. 2-3 Comparison of mechanical properties of TiC / Al-Si composites fabricated by *in situ* process from 14 μm SiC with those of 14 μm SiC / Al-Si and 1 μm TiC / Al-Si composites fabricated by melt stirring method.

the present work are higher than those obtained by the gas injection method as indicated by broken lines[1)]. However, the values of ultimate tensile strength and 0.2 % proof stress at Vf = 10 % are lower than those at Vf = 5.5 %. This may be due to the over-ageing, because, although the hardnesses of matrix and composite at Vf = 5.5 % reached maximum values at about 86 ks aging, the time required to reach maximum hardness of composite at Vf = 10 % is shortened to about 38 ks.

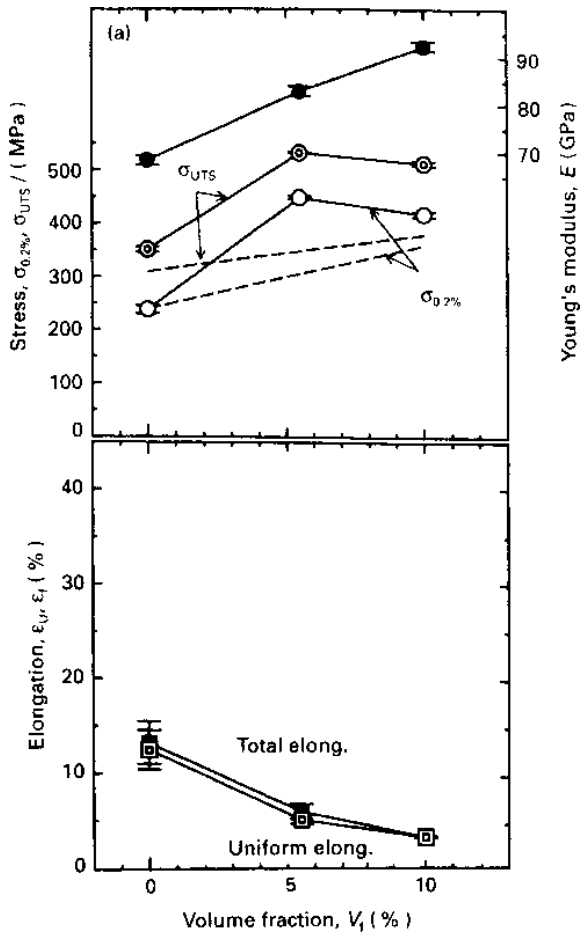


Fig. 2-4 Effect of the particulate volume fraction on the mechanical properties of *in situ*-formed TiC / Al-4.5 wt % Cu composite after T6 heat treatment, comparing with that fabricated by the gas injection method described by broken line[1].

## 2.4 Conclusions

*In situ*-formed carbide particulate-reinforced aluminum composites were fabricated by using SiC and $Al_4C_3$. The dispersion behavior of *in situ*-formed particles and the mechanical properties were investigated.

(1) Fine TiC particles of 1 μm in diameter were *in situ* formed even by using 14 μm SiC. However, the finer the raw carbide of SiC and $Al_4C_3$ were, the greater was the uniform dispersion of *in situ*-formed particle and the more the mechanical properties of composite were improved.

(2) The mechanical properties of the *in situ*-formed TiC / Al-5 mass % Cu composite after T6 heat treatment were better than those fabricated by the gas-injection method.

## References

1) P. Sahoo and M. J. Koczak, Mat. Sci. Eng., A131, (1991), 69.
2) H. Nakata, T. Choh and N. Kanetake: J. Mater. Sci., 30 (1995), 1719.
3) M. Kobashi and T. Choh, J. Japan Inst. Met., 55 (1991), 731.

## 3. Synthesis of Boride and Nitride Ceramics in Molten Aluminum by Reactive Infiltration

### 3.1 Introduction

The BN / Al system is known to be extremely reactive at temperatures higher than 1373 K[1]. So, in this work, attempts were made to fabricate ceramic / metal *in situ* composites by the spontaneous infiltration of BN-Ti and BN-Ta powder blends with molten aluminum[2], expecting following *in situ* reactions: $Ti + 2BN + 2Al \rightarrow TiB_2 + 2AlN$ and $Ta + 2BN + 2Al \rightarrow TaB_2 + 2AlN$[2].

### 3.2 Experimental procedure

Starting materials were titanium powder (99.8 % Ti, under 44 μm), tantalum powder (99.9 % Ta, under 44 μm), hcp-BN flake (99.9 % BN, 10 μm in diameter, 1~2 μm in thickness) and a pure aluminum ingot (99.99 % Al). The titanium or tantalum powder was blended with BN (mole ratio; Ti or Ta : BN = 1 : 2, expressed by [Ti or Ta + BN]). The loose powder blend (3 g) was placed in an $Al_2O_3$ crucible (inner diameter: 13 mm), and an aluminum ingot (15 g) was put above the loose powder blend as shown in Fig. 3-1. The specimen was then heated to 1473 K in an induction furnace, and held for 300~3600 s under a nitrogen atmosphere. After solidification, the specimen was sectioned, observed by EPMA and analyzed by XRD. Powder blend compacts were also submitted to the differential thermal analysis (DTA). The analysis was performed in an argon atmosphere

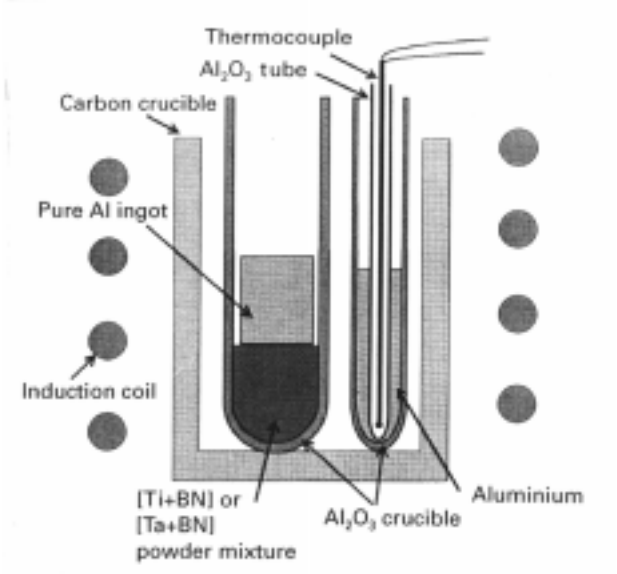


Fig. 3-1 A schematic illustration of the experimental setup.

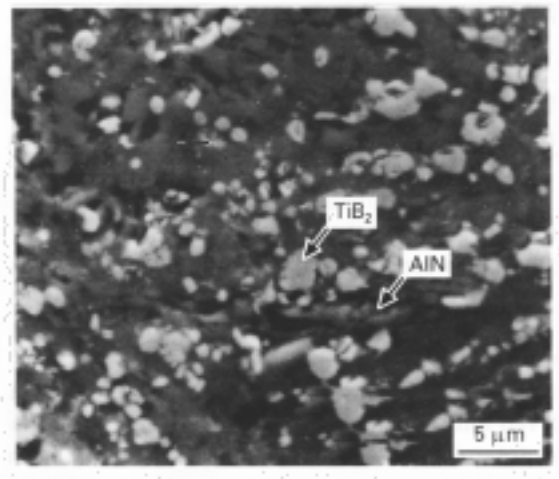


Fig. 3-2 A secondary electron image of the cross-section of composite fabricated from the [Ti + BN] powder blend infiltrated with the molten aluminum and held for 3600 s at 1473 K.

with a heating rate of 10 K/min.

## 3.3 Results and discussion

### 3.3.1 *Observation of miocrostructure*

The molten aluminum completely infiltrated into the [Ti + BN] and the [Ta + BN] powder blends by holding for 3600 s at 1473 K. In XRD pattern of these composites, strong peaks of $TiB_2$ and AlN, or $TaB_2$ and AlN were detected, whereas the peaks of BN were rarely detected, indicating that the BN and titanium or tantalum were completely converted to $TiB_2$ or $TaB_2$ and AlN during the 3600 s hold at 1473 K. Fig. 3-2 shows a microstructure of the composite fabricated from the [Ti + BN] powder blend held for 3600 s. $TiB_2$ and AlN particles are clearly visible. In microstructures of composite fabricated from the [Ti + BN] powder blend held for 1800 s, however, residual $Al_3Ti$ and BN were visible and $TiB_2$ particles formed could be identified at the interface between BN and molten aluminum, indicating that the *in situ* reaction was still in progress after a 1800 s hold. Conversely, specimen from the [Ta + BN] powder blend showed a complete conversion of the starting materials to $TaB_2$ and AlN even with a short 300 s hold.

### 3.3.2 *Infiltration process analysis*

The temperature of the powder phase during the fabrication process was measured by inserting a thermocouple into the crucible. Figure 3-3 shows the temperature profile of the [Ti + BN] powder blend as a function of processing time. The temperature increased steadily during the heating process up to 1420 K. The temperature rose sharply at 1420 K and reached a peak value of 1670 K. Although the temperature profile for the [Ta + BN] powder blend, shown in Fig. 3-4, was also measured in the same way, the maximum temperature reached by the exothermic reaction could not be measured, owing to the damage of the thermocouple caused by contacting with molten aluminum. The typical difference in the temperature profile of the two systems are as follows: the infiltration and the exothermic reaction take place simultaneously for the [Ti + BN] powder blend, whereas there is an incubation period for the [Ta + BN] powder blend.

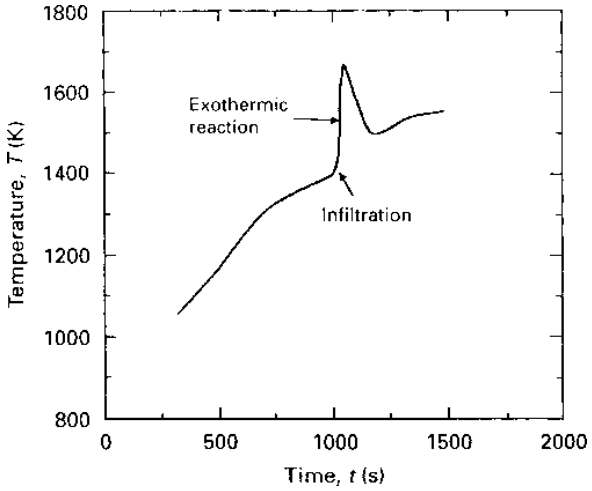


Fig. 3-3 A schematic representation of the temperature-time curve during the infiltration process for the [Ti + BN] powder blend.

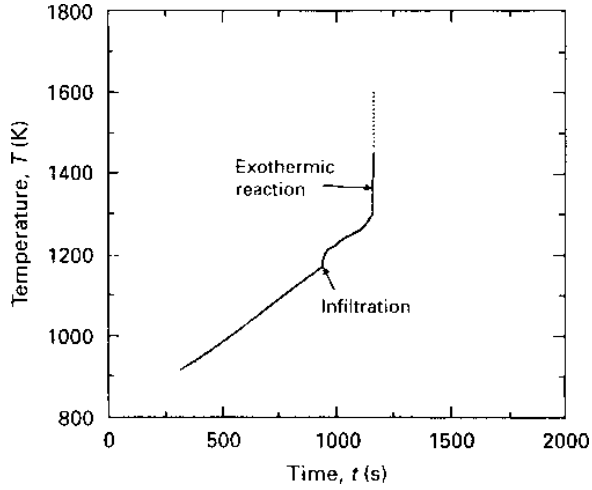


Fig. 3-4 A schematic representation of the temperature-time curve during the infiltration process for the [Ta + BN] powder blend.

Then, the maximum attainable temperature of the [Ti + BN] powder blend during the infiltration was calculated assuming that the $Al_3Ti$ is produced immediately after the infiltration. The constituents of the system changes before and after the infiltration as follows; before infiltration: [Ti + 2BN + (3+$x$)Al] and after infiltration: [$Al_3Ti$ + 2BN + $x$Al], where $x$ is a mole amount of excess aluminum after the formation of the $Al_3Ti$. Since the porosity of the [Ti + BN] powder blend was 70 vol %, a value of $x$ in this case was calculated to be 4.7 mol. The adiabatic temperature ($T_{ad}$) was then calculated using the following equation;

$$\Delta H_{f,Al_3Ti} + 4.7\int_{T_0}^{T_m} C_{P,Al}\,dT + 2\int_{T_0}^{T_m} C_{P,BN}\,dT + \int_{T_0}^{T_m} C_{P,Al_3Ti}\,dT$$
$$+ V_D\Delta H_{D,Al_3Ti} + 6.7\int_{T_m}^{T_l} C_{P,Al}\,dT + 2\int_{T_m}^{T_l} C_{P,BN}\,dT + \int_{T_m}^{T_l} C_{P,TiAl}\,dT = 0$$

where $\Delta H_f$ is heat of formation, $C_p$ is specific heat, $T_m$ is the decomposing temperature of $Al_3Ti$ (1613 K), $V_D$ is the mole amount of decomposed $Al_3Ti$ at 1613 K and $\Delta H_D$ is an enthalpy change of the $Al_3Ti$ decomposition. Since the initiating temperature ($T_0$) of the reaction is confirmed to be 1420 K from Fig. 3-3, the adiabatic temperature ($T_{ad}$) was calculated to be 1660 K. The calculated adiabatic temperature shows a close agreement with the measured maximum temperature (1670 K). This indicates that the sharp increase in temperature of [Ti + BN] powder blend shown in Fig. 3-3 was caused by the $Al_3Ti$ formation.

### 3.3.3 *In situ reaction analysis by DTA*

To analyze the reaction process, a differential thermal analysis was performed for four powder blends. DTA curves of the [Ti + BN + Al] and [Ti + Al] powder blends are shown in Fig. 3-5. A strong exothermic peak at 1030 K (peak-B) and a broad peak at around 1300 K (peak-C) were detected in the [Ti + BN + Al] powder blend. A strong exothermic reaction (peak-E) was also detected in the [Ti + Al] powder blend. The endothermic peak-D indicates melting of aluminum and, therefore, the peak-E and the peak-B are regarded as being the formation of titanium aluminide (TiAl, $Ti_3Al$ and/or $TiAl_3$). On the other hand, the DTA curves of the [Ta + BN + Al] and [Ta + Al] powder blends reveal an incubation period between peak-F and peak-G, and between peak-H and peak-I, respectively (Fig. 3-6). Hence, when the [Ta + BN] powder blend was used, the reaction producing $Al_3Ta$ was not observed. However, an over-all reaction between tantalum, aluminum and BN occurred at a time after the incubation period. Conversely, when the [Ti + BN] powder blend was used, the formation of $Al_3Ti$ occurs immediately after the infiltration. The formation of

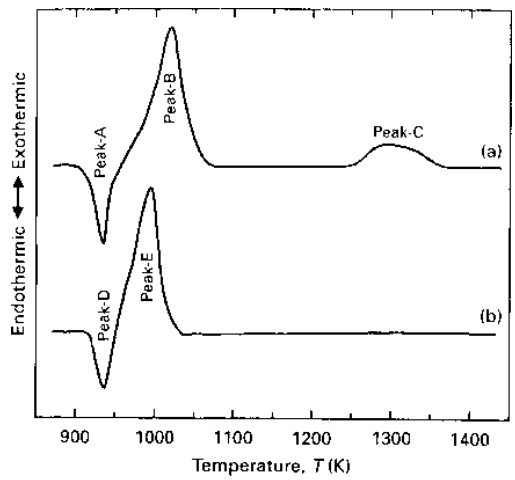


Fig. 3-5 Differential thermal analysis curves obtained from (a) the [Ti + BN + Al] and (b) [Ti + Al] powder blends.

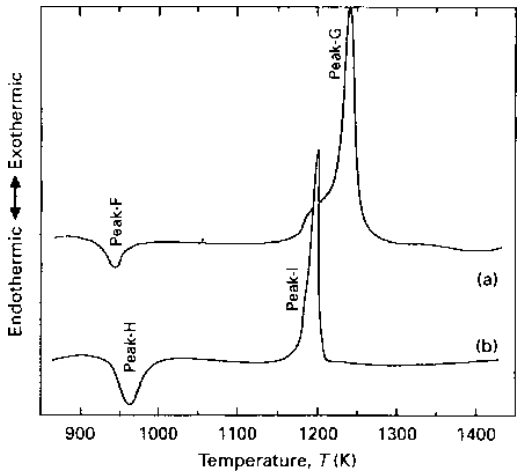


Fig. 3-6 Differential thermal analysis curves obtained from (a) the [Ta + BN + Al] and (b) [Ta + Al] powder blends.

$TiB_2$ particles should occur through the decomposition of $Al_3Ti$ at around 1300 K (peak C). Therefore, the conversion of BN to $TiB_2$ and AlN takes a longer time than that of BN to $TaB_2$ and AlN.

## 3.4 Conclusions

The [Ti + BN] and [Ta + BN] powder blends were infiltrated with molten aluminum at 1473 K to produce ceramic / metal composites. Results obtained here are summarized as follows.

(1) Both [Ti + BN] and [Ta + BN] powder blends were completely infiltrated by molten aluminum held for 3600 s at 1473 K, and then $TiB_2$ and AlN, and $TaB_2$ and AlN were formed, respectively.

(2) According to DTA, the [Ti + BN + Al] powder blend showed two exothermic reactions, whereas the [Ta + BN + Al] powder blend showed only one exothermic reaction.

(3) The $Al_3Ti$ forming reaction took place immediately after the infiltration of the [Ti + BN] powder blend, but the reaction forming both $TiB_2$ and AlN proceeded gradually. The time required to complete the $TiB_2$ and AlN formation was in a range of 1800~3600 s.

(4) There was an incubation period for [Ta + BN] / Al system. The over-all reaction between tantalum, aluminum and BN took place after the incubation period. The time required to complete the $TaB_2$ and AlN formation was less than 300 s.

## References

1) S. J. Park, H. Fujii and H. Nakae: J. Jap. Inst. Met., 58 (1994), 208.
2) M. Kobashi and T. Choh: J. Mater. Sci., 32 (1997), 6283

## 4. Synthesis of AlN / Al Alloy Composites by *In Situ* Reaction between $Mg_3N_2$ and Aluminum

### 4.1 Introduction

The fabrication of AlN / Al composites with the help of the *in situ* reaction between molten aluminum and nitrogen-containing gases were previously reported[1),2)]. However, these techniques took relatively long time (several hours). In the present work[3)], a reaction between molten aluminum and a solid nitride of $Mg_3N_2$ was employed to synthesize AlN through following reaction: $Mg_3N_2 + 2Al \rightarrow 2AlN + 3Mg$. The benefits of using solid nitride powders instead of using gas phases are basically twofold of (1) the synthesis of AlN in a short time and (2) controlling the morphology of AlN from discrete to three dimensionally continuous.

### 4.2 Experimental procedure

An experimental setup for the spontaneous infiltration is the same as that shown in the chapter 3. A 3.0 g of $Mg_3N_2$ powders (either loose or compacted powders: diameter: 16 mm) was located in a cylindrical alumina crucible. An aluminum ingot (99.99 % Al, 13 g) was put on the $Mg_3N_2$ powder layer. The specimen was heated up to 1473 K and held for 3600 s under a nitrogen atmosphere. Vertical cross sections of the specimen were observed and analyzed by SEM, EPMA and XRD. The porosity of $Mg_3N_2$ powder layer was 66.2 vol % and 33.4 vol % for loose and compacted powders, respectively. As a consequence of the *in situ* reaction, the composition of the matrix alloy becomes Al-16 mass % Mg. The powder blend compacted (mole ratio; Al : $Mg_3N_2$ = 2:1) was submitted to DTA equipment. The analysis was conducted in an argon atmosphere with a heating rate of 0.167 K / s.

### 4.3 Results and discussion

#### 4.3.1 *Microstructure*

An optical micrograph of the specimen's vertical cross section revealed the complete infiltration. In the composite, the volume fraction of AlN was calculated to be 21.0 % on an assumption that $Mg_3N_2$ was fully converted to AlN. By an X-ray diffraction profile of the composite, the X-ray peaks of AlN were detected, whereas those of $Mg_3N_2$ were rarely detected. Hence, $Mg_3N_2$ was confirmed to change to AlN by the given processing condition. The microstructure of the specimen observed by SEM and EPMA is shown in Fig. 4-1, indicating that, although the average diameter of AlN was observed in the range of 5–50 μm, the observation with a higher magnification showed the AlN made up of finer discrete AlN particles(average size: 0.1–0.5 μm) *in situ* produced from loose powders. Aiming at increasing the volume fraction of AlN and producing interpenetrating-type AlN / Al composites, a $Mg_3N_2$ powder compact was used as a starting material. Fig. 4-2 shows a vertical cross section of the specimen produced under the same condition. The complete infiltration without pores was confirmed. The volume fraction of AlN is calculated to be 57.4 %. By the analysis of SEM and EPMA, the dark part was identified as AlN and bright part was identified as a residual Al-Mg alloy. The microscopic observation after dissolving residual aluminum alloy by an acid revealed the matrix made up of three dimensionally connected fine AlN particles.

#### 4.3.2 *Analysis of reaction*

Figure 4-3 shows a DTA curve. The first endothermic peak indicates the fusion of aluminum. The only exothermic peak, initiating at around 1150 K, is considered to indicate the formation of AlN, because the specimen showed a microstructure containing AlN. Figure 4-4 shows a tempera-

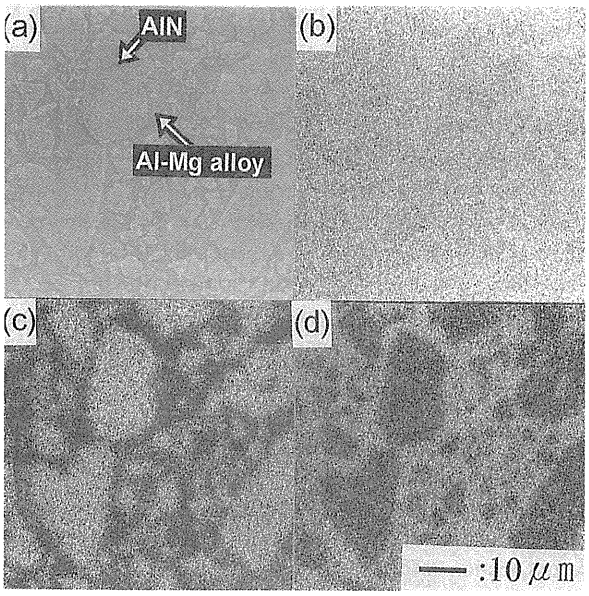


Fig. 4-1 (a) A scanning electron micrograph and X-ray images of (b) aluminum, (c) nitrogen and (d) magnesium.

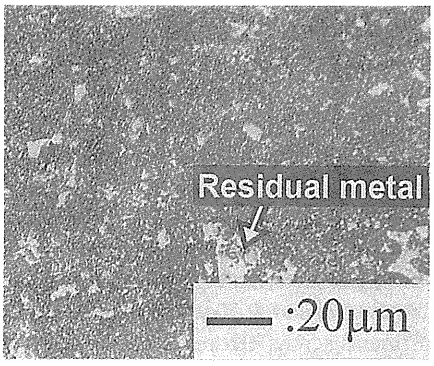


Fig. 4-2 A scanning electron micrograph of a specimen synthesized from a $Mg_3N_2$ powder compact.

ture profile of loose $Mg_3N_2$ powders measured by a thermocouple embedded in the crucible. The x-axis shows the holding time at 1473 K. A sharp exothermic peak was identified at a holding time of 770 s, proving that the *in situ* reaction occurred during holding with the temperature raising up to 1840 K. It is noticeable that the initiation temperature of the reaction obtained from the infiltration (1473 K) was inconsistent with the DTA result (1150 K). This is because the aluminum ingot used was covered with the oxide film, which hindered the direct contact of molten aluminum with $Mg_3N_2$ powders, whereas the DTA specimen compressed was in direct contact with each other.

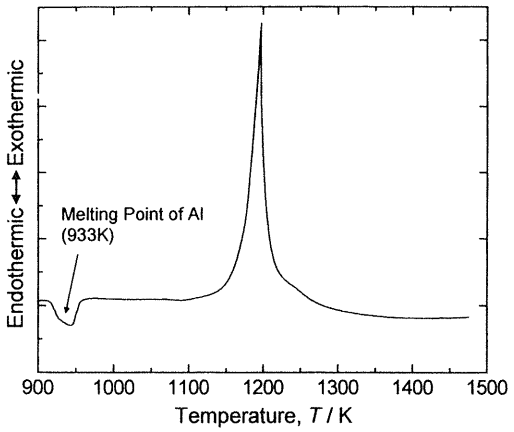


Fig. 4-3 A differential-thermal-analysis curve obtained from the [$Mg_3N_2$ + Al] powder compact. (Mole mixture ratio of $Mg_3N_2$: Al is 1:2.)

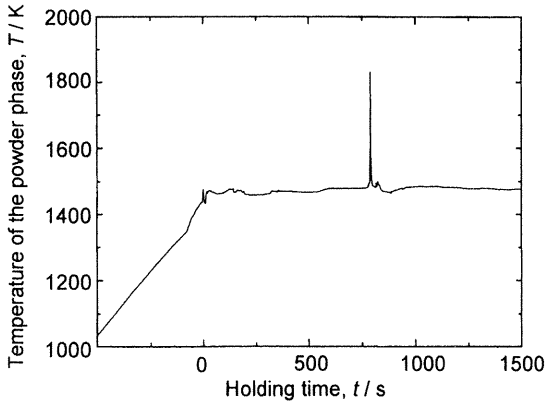


Fig. 4-4 A temperature profile of the loose $Mg_3N_2$ powder phase during the processing period as a function of the holding time at 1473 K.

### 4.3.3 *Adiabatic temperature*

If the peak temperature caused by the reaction exceeds the melting point of AlN, molten AlN tends to form a thin continuous film and, after solidification, the solid film prevents the further infiltration[4]. Therefore, in order to obtain the perfect infiltration, it is important that the peak temperature does not exceed the melting point of AlN (3073 ± 50 K). To begin with, an adiabatic temperature ($T_{ad}$) was calculated for the loose powders by using the following equation:

$$2\Delta H_{f,AlN} + \int_{T_0}^{T_{ad}} \left(2C_{P,AlN} + 3C_{P,Mg} + 4.98C_{P,Al}\right)dT + \left(\Delta H_{b,Mg}\right) = 0$$

where, $\Delta H_{f,AlN}$ is an enthalpy change for the formation of AlN, $T_0$ is an initial temperature (1473

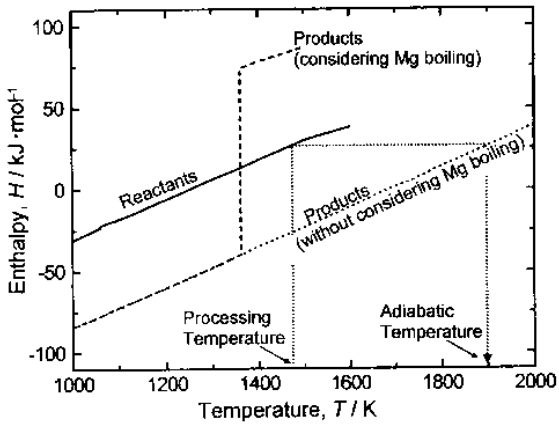


Fig. 4-5 Enthalpy data of the reactants and products as a function of temperature, showing an adiabatic temperature caused by the reaction.

K), $C_p$ is a heat capacity and $\Delta H_{b,Mg}$ is an enthalpy change of magnesium from liquid to vapor. Calculations were carried out on two basis, i.e., with and without considering the evaporation of magnesium. Figure 4-5 shows enthalpy data of reactants ($Mg_3N_2$ and Al) and products (AlN and Al). From Fig. 4-5, following results are clear: (a) If magnesium released from $Mg_3N_2$ evaporates just after the reaction, the temperature of the system does not elevate because the heat of reaction was completely consumed by the latent heat of evaporation, (b) If magnesium is assumed not to evaporate but to diffuse into molten aluminum, the adiabatic temperature raises up to 1900 K. In the practical measurement shown in Fig. 4-4, the maximum temperature was 1840 K, which shows a good agreement with the calculated result based on the assumption that magnesium does not evaporate. Hence, magnesium is expected to diffuse into molten aluminum soon after the reaction. The calculation was also carried out for the compacted $Mg_3N_2$ powders. The adiabatic temperature was calculated as 2400 K on the assumption that magnesium does not evaporate. This temperature is still lower than the melting point of AlN, proving that the choking of infiltration paths can be avoided.

## 4.4 Conclusions

The spontaneous infiltration of the $Mg_3N_2$ powders with molten aluminum and the subsequent *in situ* reaction between these materials were investigated. The main results were as follows.

(1) Molten aluminum infiltrated into $Mg_3N_2$ powders spontaneously. Neither large pores nor non-infiltrated regions were visible.

(2) As a result of the *in situ* reaction, AlN was synthesized in a molten Al-Mg alloy.

(3) The volume fraction of AlN was roughly controlled by changing packing densities of $Mg_3N_2$ powders. By decreasing the porosity in $Mg_3N_2$ powders from 66.2 vol % to 33.4 vol %, morphology of AlN shifted from discrete to continuous.

(4) DTA curve showed a sharp exothermic peak initiating at around 1150 K.

(5) A sharp increase in the temperature of loose $Mg_3N_2$ powders infiltrated with molten aluminum was observed during the holding period at 1473 K. The maximum peak of the temperature profile (1840 K) agreed well with the calculated adiabatic temperature (1900 K).

## References

1) P Sahoo and M. J. Koczac: Mater. Sci. Eng., A144 (1991), 37.
2) H. Scholz and P. Greil: J. Mater. Sci., 26 (1991), 669.
3) M. Kobashi, N. Okayama and T. Choh: Mater. Trans. JIM, 38 (1997), 260
4) M. Kobashi, N. Okayama and T. Choh: J. Mater. Sci., 32 (1997), 6279

## 5. An *In Situ* $TiB_2$ / Al Composite Fabricated from TiN, $TiC_xN_{1-x}$ and Boron Powders by Reactive Infiltration of Molten Aluminum

### 5.1 Introduction

The aim of the present work is to study an *in situ* reaction taking place between TiN or $TiC_xN_{1-x}$, boron powder and molten aluminum during reactive infiltration to fabricate a $TiB_2$ / Al composite[1)].

### 5.2 Experimental procedure

The average particle size of TiN, $TiC_{0.3}N_{0.7}$, $TiC_{0.5}N_{0.5}$, $TiC_{0.7}N_{0.3}$ and boron powders used in this work was –44, 1.48, 1.31, 1.32 and –149 μm, respectively. An aluminum or Al-10 wt % Mg alloy ingot (10g) was set on the [TiN or $TiC_xN_{1-x}$ + B] powder blend (5.5 g) in an alumina crucible. Then, under an argon atmosphere, the specimen was heated to 1000 or 1200˚C, held for 3600 s in an induction furnace, and finally quenched in water. The specimens were sectioned and examined by EPMA and XRD. DTA was also performed. Another setup shown in Fig. 5-1 was used to record temperature profile of the powder blend during infiltration by inserting three thermocouples into the powder blend. The crucible containing powder-ingot pair and attached thermocouples was then heated to 1200˚C at a rate of 7.5˚C/min under an argon in an infrared image furnace.

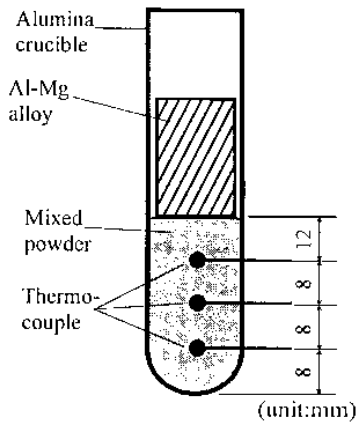


Fig. 5-1 Experimental setup used to measure infiltration rate

## 5.3 Results and discussion

Neither pure aluminum nor Al-10 mass % Mg alloy infiltrated into the powder blend at 1000°C. However, at 1200°C, the Al-Mg alloy infiltrated into the powder blends, whereas pure aluminum did not. This may be due to improving the wettability by alloying magnesium[2), 3)].

The XRD patterns of the infiltrated composites are shown in Fig. 5-2. *In situ*-formed $TiB_2$ and AlN particles are detected in the composites in all cases. No TiN is also seen in the composite fabricated from the [TiN + B] / Al-Mg system (Fig. 5-2(a)), while some $TiC_xN_{1-x}$ residue are observed in other composites as shown in Fig. 5-2(b)-(d). These indicate that the reaction between TiN, boron and aluminum melt was complete, whereas that between $TiC_xN_{1-x}$, boron and aluminum was not complete. The amount of *in situ*-formed particles increases with the decrease in the x-value of $TiC_xN_{1-x}$ contained in the starting powder blend. Although the *in situ*-formed particles fabricated from the [$TiC_xN_{1-x}$ + B] / Al-Mg system was detected in the composite by XRD patterns, those particles could hardly be observed by EPMA, because they were very fine owing to incomplete reaction. On the other hand, $TiB_2$ particles formed from the [TiN + B] / Al-Mg system

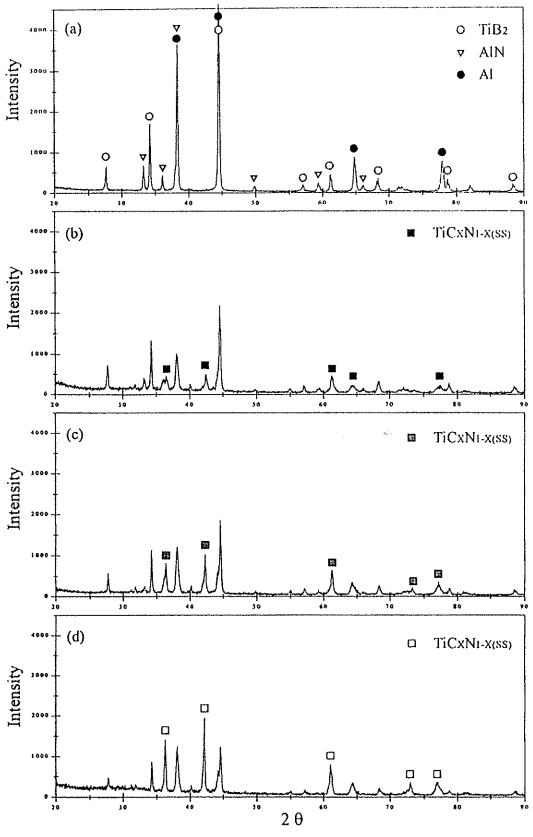


Fig. 5-2 The X-ray diffraction pattern for the composites fabricated from (a) [TiN + B], (b) [$TiC_{0.3}N_{0.7}$ + B], (c) [$TiC_{0.5}N_{0.5}$ + B] and (d) [$TiC_{0.7}N_{0.3}$ + B] powder blends infiltrated with Al-Mg alloy, and held for 1 hour at 1200°C.

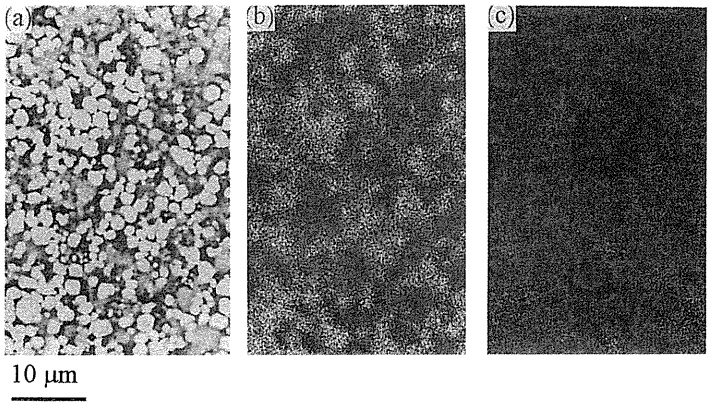


Fig. 5-3 (a) back scattered electron micrograph and X-ray image of (b) titanium and (c) boron of the composite fabricated from the [TiN + B] powder blend infiltrated with Al-Mg alloy, and held for 1 hour at 1200°C.

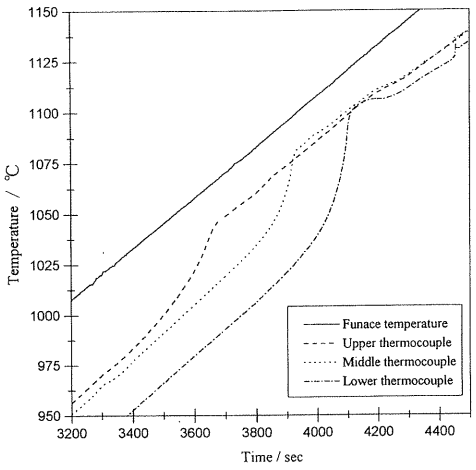


Fig. 5-4 Schematic illustration of the temperature-time curves during the infiltration process of the [$TiC_{0.7}N_{0.3}$ + B] powder blend with molten Al-Mg alloy.

could be detected in the composite by EPMA as shown in Fig. 5-3. Furthermore, AlN particles was visible in this composite, but the x-ray intensity of nitrogen was too weak for printing.

DTA measurement revealed an exothermic peak at around 1050°C in all cases except for the [TiC + B + Al] powder blend. These peaks are related with a following reaction between the starting powders and the melt as: $TiN + 2B + Al = TiB_2 + AlN$.

The dotted curves shown in Fig. 5-4 indicate the typical temperature profiles for the [$TiC_{0.7}N_{0.3}$ + B] powder blend during spontaneous infiltration with an Al-10 mass % Mg melt. It is apparent that each curve has a temperature peak showing nearly simultaneous infiltration and exothermic reaction taking place between the starting powder and the melt to start at around 1050°C. The

average infiltration rates obtained by using the time lag between the maximum point of peaks during infiltration increased with the decrease in the x-value of $TiC_xN_{1-x}$ in the starting materials as given by 3.51, 5.35, 6.99 and $8.78 \times 10^{-2}$ mm/s at x = 0.7, 0.5, 0.3 and 0, respectively.

According to these results, the spontaneous infiltration seems to be controlled by the exothermic reaction to decrease the interfacial energy between the Al-Mg melt and the solid particles to such a level that spreading of the melt on the solid surface could occur[4].

### 5.4 Conclusions

The ($TiB_2$ + AlN) / Al-Mg alloy composite was fabricated from the powder blend [TiN, $TiC_xN_{1-x}$ and boron] by a reactive infiltration of Al-Mg alloy. The main results are as follows.

(1) $TiB_2$ particle was *in situ* formed in the composite by holding reaction system for I hour at 1200˚C through the infiltration process.

(2) The reactive infiltration of powder blend with molten aluminum occurred by alloying magnesium to improve the wettability.

(3) Both the amount of *in situ*-formed particles in the composite and the infiltration rate increased with the decrease in the x-value of $TiC_xN_{1-x}$.

(4) The infiltration front temperature was elevated by the exothermic reaction to enhanced the further infiltration.

## References

1) E. Taheri-Nassaj, M. Kobashi and T. Choh: Script. Met. Mater., 34 (1996), 1257.
2) E. Taheri-Nassaj, M. Kobashi and T. Choh: Scripta Metall. Mater., 32 (1995), 1923.
3) G. Lang: Aluminium, 49 (1973), 231 and 50 (1974), 731.
4) I. A. Aksay, C. E. Hoge and J. A. Pask: J. Phys. Che., 78 (1974), 1178.

## 6. An *In Situ*-Formed Boride / Al Composites Fabricated from $B_4C$ and Metal Powders by Reactive Infiltration of Molten Aluminum

### 6.1 Introduction

Reactive infiltration process offers the advantages of producing metal matrix composite with a high ceramic content and near-net-shape fabrication[1)-3)]. The aim of the present work is to study the *in situ* reactions taking place between Nb, Ta, Hf or Ti, $B_4C$ powders and aluminum during spontaneous infiltration to fabricate aluminum matrix composites reinforced with *in situ*-formed carbide and boride particles[4].

### 6.2 Experimental procedure

Starting materials used in this work was Nb, Ta, Hf, Ti and $B_4C$ powders. In the crucible, an aluminum ingot was set on the loose powder blend with the mole ratio of Nb, Ta, Hf or Ti to $B_4C$ being 3 : 1. A sample was heated to 1200˚C and held for 3600 s under a nitrogen atmosphere. The fabricated composites were sectioned and examined by XRD. Also, DTA was performed. Furthermore, to identify the phases *in situ* formed, a series of another experiments was conducted by using a pressed powder blend (15 mm diameter and 4 mm height) with the mole ratio of the metal powder to $B_4C$ and Al being 3:1:15. These specimens were heated up to the given temperature and

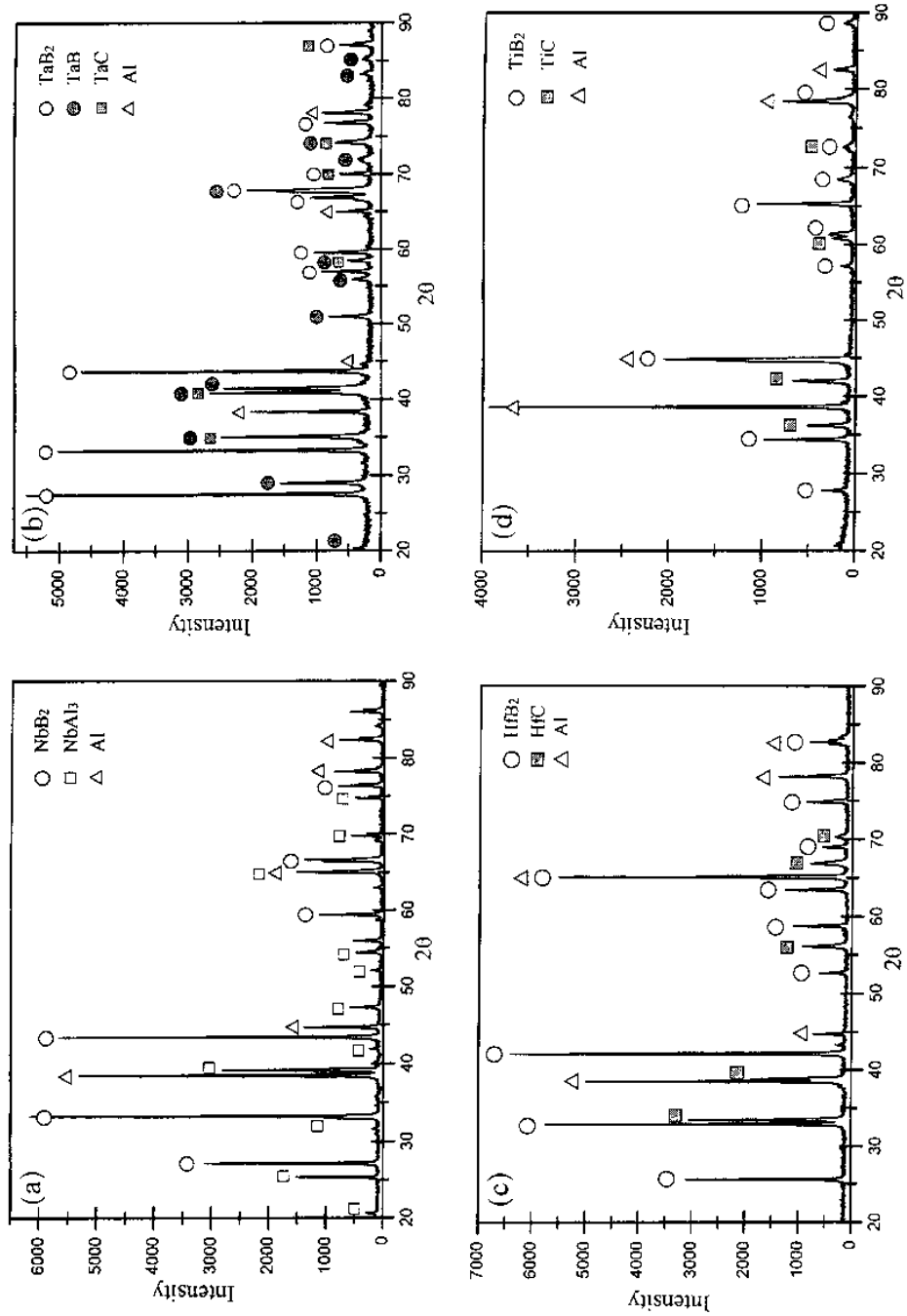


Fig. 6-1 The X-ray diffraction pattern for the fabricated composites: (a) Nb-$B_4C$ / Al, (b) Ta-$B_4C$ / Al, (c) Hf-$B_4C$ / Al and (d) Ti-$B_4C$ / Al.

quenched in water. The sectioned specimen was polished and examined by XRD.

## 6.3 Results and discussion

All powder blends were infiltrated by the pure Al melt spontaneously. The XRD patterns of the composites are also presented in Fig. 6-1, indicating that the *in situ*-formed boride and carbide are detected in all composites except for the system Nb-$B_4C$ / Al where $NbAl_3$ and $NbB_2$ were formed. DTA analyses for the powder blends are shown in Fig. 6-2. As can be seen, one or more exothermic reactions occur in all ternary powder blends. According to DTA and its relevant XRD, the first and the second exothermic peak in Ti-$B_4C$-Al system seem to correspond to the formation of $Al_3Ti$ and to the reaction: $3Al_3Ti + B_4C = 2TiB_2 + TiC + 9Al$, respectively. In Hf-$B_4C$-Al system, the first, the second and the third exothermic peak correspond to the formations of $Al_3Hf$, $Al_3Hf + HfB_2$ and $HfB_2 + HfC$, respectively. In Ta-$B_4C$-Al system, the first and second exothermic peak are related with the formations of $TaB_2 + TaB$ and $TaB_2 + TaB + Ta_3B_4 + TaC$, respectively. Nb-$B_4C$-Al system revealed only one exothermic peak which seems to be related with the formations of $NbB_2$ and $NbAl_3$. It was also shown that the formed $NbAl_3$ dissociates and then forms $NbB_2$, when a heat treatment was continued for longer time. From DTA and XRD results, it is suggested that the *in situ*-formed aluminides were dissociated in all systems and then forms the *in situ* borides and/or carbides by a heat treatment with higher temperature or longer time except for the Ta-$B_4C$-Al in which $TaAl_3$ was not formed. This is maybe due to a very higher affinity of Ta to boron than to aluminum. It is also seen that no NbC is formed in Nb-$B_4C$-Al system shown in Fig. 6- 1. This is maybe because of a higher affinity of Nb to boron than to carbon.

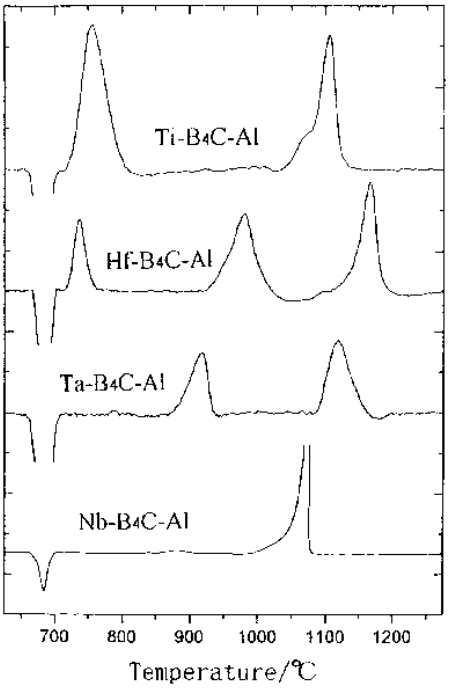


Fig. 6-2 Differential thermal analysis curves obtained from four powder blends.

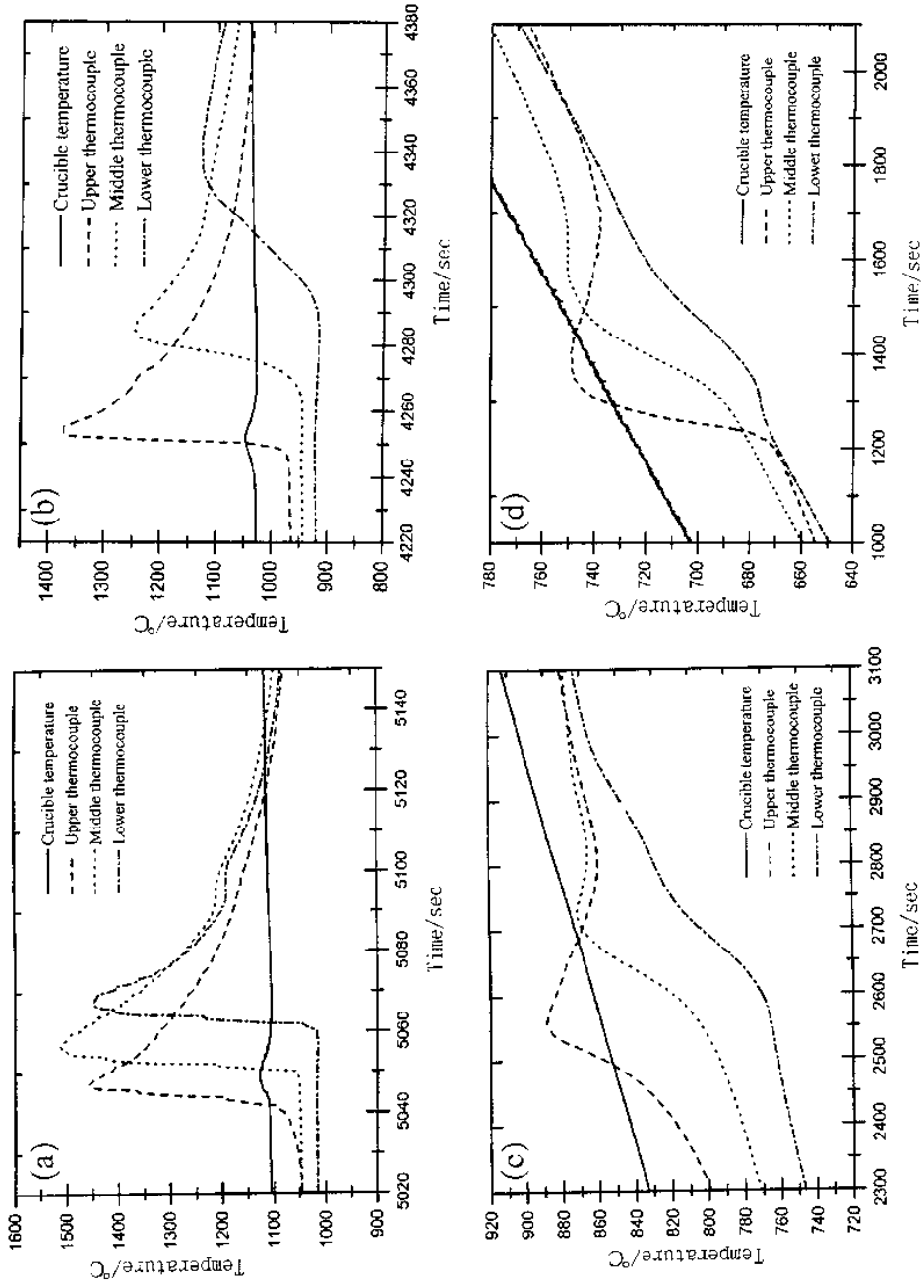


Fig. 6-3 Schematic representation of the temperature-time curves during the infiltration process for (a) Nb-$B_4C$ / Al, (b) Ta-$B_4C$ / Al, (c) Hf-$B_4C$ / Al and (d) Ti-$B_4C$ / Al systems.

Figure 6-3 shows the temperature profiles for these powder blends during spontaneous infiltration by a molten aluminum. It is seen that each curve has a peak showing nearly simultaneous infiltration and exothermic reactions in the infiltration front. Hence, it is suggested that the infiltration is driven by the exothermic reactions between the starting powders and the melt. Furthermore, as well as the average infiltration rate, the start point of elevating temperature regarded as being an infiltration threshold temperature and the peak of the elevated temperature regarded as an infiltration front temperature decrease in all, in order of Nb-, Ta-, Hf- and Ti-$B_4C$ / Al systems, probably according to increasing aluminide formation tendency belonging to the blended metal.

### 6.4 Conclusions

A reactive infiltration was used to fabricate an aluminum matrix composite reinforced with boride and carbide particles by using Nb, Ta, Hf or Ti, $B_4C$ powders and aluminum ingot. The main results are as follows.

(1) Powder blends of Nb-$B_4C$, Ta-$B_4C$, Hf-$B_4C$ and Ti-$B_4C$ were spontaneously infiltrated by an aluminum melt.

(2) $NbB_2$, $TaB_2$, $HfB_2$ and $TiB_2$ were in situ formed by exothermic reactions.

(3) The infiltration was maybe driven by the exothermic reaction taking place between the starting powder and the melt.

(4) The infiltration rate was seen to increase with increasing temperature of the infiltration front.

## References

1) D. C. Dunand, J. L. Sommer and A. Mortensen: Metall. Trans., 24A (1993), 2161.
2) D. Muscat and R. A. L. Drew: Metall. Mater. Trans., 25A (1994), 2357.
3) A. Mortensen and J. A. Cornie: Metall. Trans., 18A (1987), 1160.
4) E. Taheri-Nassaj, M. Kobashi and T. Choh: Scripta Mater., 37 (1997), 605.

## 7. Fabrication of Particulate Reinforced Magnesium Composites by Spontaneous Infiltration

### 7.1 Introduction

Magnesium matrix composites have various advantages such as low specific weight, high specific strength, high elastic modulus and high wear resistance. In the present work, an attempt was made to fabricate SiC particulate reinforced magnesium composite by applying a spontaneous infiltration of the molten magnesium into the SiC powder phase blended with $SiO_2$ particles[1)].

### 7.2 Experimental procedure

Starting materials used in this work are magnesium (99.97 %), $SiO_2$ powder (2 $\mu$m) and SiC powders (1.2–8.0 $\mu$m). A pure magnesium ingot (4 g) was set on the [SiC + $SiO_2$] powder blend (1.6 g) in a crucible with small two holes at the bottom. A sample was heated to 973 K and held for 20 min under an argon atmosphere in an induction furnace. After cooling, the sample was sectioned and examined by EPMA and XRD. The infiltration-front temperature and the infiltration velocity were measured by setting three thermocouples similarly as previously mentioned.

## 7.3 Results and discussion

### 7.3.1 *Spontaneous infiltration and microstructure*

The $SiO_2$ content in the powder blends necessary for inducing spontaneous infiltration was measured for various SiC diameters. The results are shown in Fig. 7-1, where complete infiltration, incomplete infiltration and no infiltration are denoted by ○, △ and ×, respectively. A broken line was drown on the boundary between the complete and the incomplete infiltration systems. This result suggests that the $SiO_2$ content necessary for the complete infiltration increases with the decease in the SiC diameter. Finally, into the [1.2 μm SiC + $SiO_2$] powder blend, molten magnesium cannot spontaneously infiltrate even if $SiO_2$ powder were blended up to 31 mass %. In this case, therefore, the $SiO_2$ content required for the spontaneous infiltration must increase to the

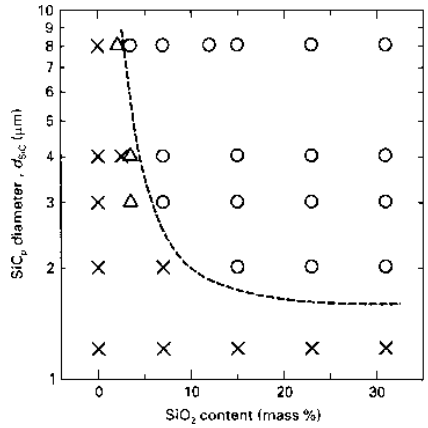


Fig. 7-1 Effects of $SiO_2$ content and SiC particle diameter on the spontaneous infiltration.

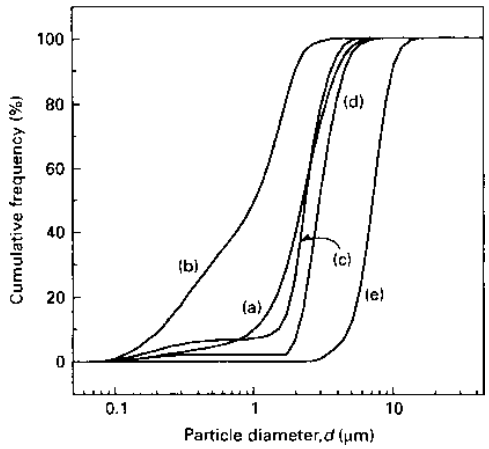


Fig. 7-2 Particle diameter distributions of (a) $SiO_2$ and (b)-(e) SiC particles: (b) 1.2, (c) 2, (d) 3 and (e) 8 μm.

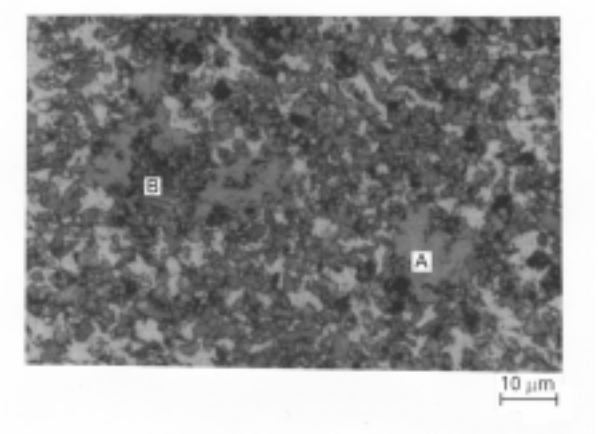


Fig. 7-3 Microstructures of composite fabricated by the spontaneous infiltration of the [3 μm SiC + 7 mass % $SiO_2$] powder blend with molten magnesium.

considerable high level, because the particle diameter distributions of 1.2 μm SiC is smaller than that of $SiO_2$ in all range as shown in Fig. 7-2, indicating cumulative frequency (%) of the diameter for each particle. Hence, below 31 mass % $SiO_2$, the $SiO_2$ powder blended in the 1.2 μm SiC particles may be surrounded with the inactive smaller SiC particles and be prevented from the direct contact with the magnesium melt, resulting in no infiltration.

The microstructure of composite fabricated from the [3 μm SiC + 7 mass % $SiO_2$] / Mg system is shown in Fig. 7-3, indicating the uniform distribution of the SiC particles blended and two reaction products of A and B formed during the infiltration. By EPMA and XRD analyses, A and B are regarded as being $Mg_2Si$ and MgO, formed by the following reaction: $4Mg + SiO_2 = Mg_2Si + 2MgO$.

### 7.3.2 *Infiltration-front temperature and infiltration velocity*

By measuring the temperature profile of the powder blend during the infiltration, it was detected that the temperature at the infiltration front was higher than elsewhere. Hence, it is considered that spontaneous infiltration occurs under the good wettability condition induced by the elevated temperature at the infiltration front caused by Mg-$SiO_2$ reaction. To confirm this effect, the spontaneous infiltration of pure SiC with the magnesium melt was tried at higher temperature of 1273 K. Consequently, spontaneous infiltration occurred, although many defects were included. Figure 7-4 shows the relation between the infiltration-front temperature, the $SiO_2$ content and the SiC diameter. According to Fig. 7-4, the infiltration-front temperature increases linearly with increasing $SiO_2$ content and decreases with decreasing SiC diameter. Furthermore, the infiltration velocity is also influenced by both the $SiO_2$ content and the SiC diameter as shown in Fig. 7-5. Concerning the SiC diameter, the velocity increases with increasing SiC diameter below 15 mass % $SiO_2$. This phenomenon seems to depend on the hydraulic radius, r, that can be calculated by the following equation: $r = d\phi/[6\lambda(1-\phi)]$ , where d is the average particle diameter, $\phi$ is the porosity, and $\lambda$ is the geometry factor (= 1.42[2)]). The hydraulic radius was calculated by neglecting the existence of $SiO_2$ blended in the powder, because it is consumed by magnesium. The calculated results inferred that hydraulic radius increases with increasing SiC diameters, suggesting a good agreement with the experimental results: e.g. in 15 mass % $SiO_2$, the radii estimated were 1.0, 1.5, 1.8 and 3.1 $\mu$m for 2, 3, 4 and 8 $\mu$m in the diameter of the SiC, respectively. However, the behavior

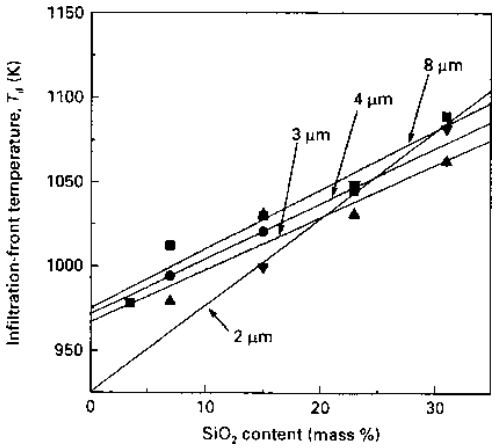


Fig. 7-4 Effects of $SiO_2$ content and SiC particle diameter on the infiltration-front temperature. SiC diameter; ( ■ ): 8 μm, ( ● ): 4 μm, ( ▲ ): 3 μm, ( ▼ ): 2 μm.

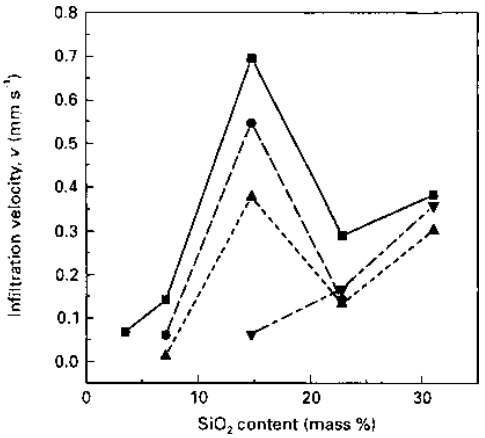


Fig. 7-5 Effects of $SiO_2$ content and SiC particle diameter on the infiltration rate. SiC diameter; ( ■ ): 8 μm, ( ● ): 4 μm, ( ▲ ): 3 μm, ( ▼ ): 2 μm.

of infiltration velocity above 15 mass % $SiO_2$ cannot be explained from this point of view.

On the other hand, the effect of $SiO_2$ content is complex as shown in Fig. 7-5, indicating that the infiltration velocity increases with increasing $SiO_2$ content until 15 mass % $SiO_2$ and then steeply decreases, probably because of the presence of the reaction products. In the infiltration process, MgO may crystallize just after reaction near the infiltration front, because of high melting point. Therefore, the formation of MgO seems to be one factor to decrease the infiltration velocity. Furthermore, the crystallization of $Mg_2Si$ taken place near the infiltration front could be confirmed by quenching [3 $\mu$m SiC + 23 mass % $SiO_2$] / Mg system during infiltration. Then, on the Mg-Si phase diagram, the measured infiltration-front temperature were plotted against the average silicon content released from $SiO_2$ by the $SiO_2$-Mg reaction as shown in Fig. 7-6. From this figure, it is

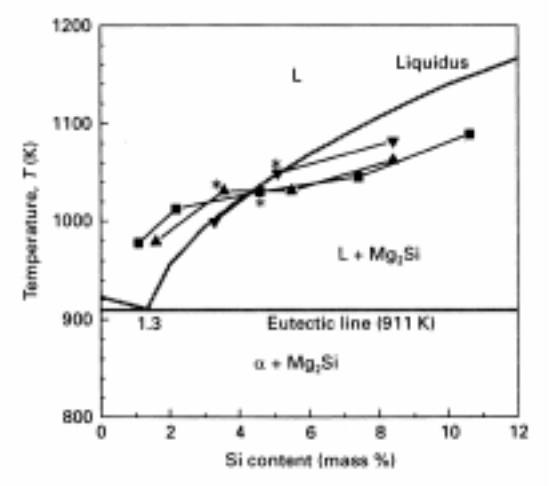


Fig. 7-6 The plot of measured infiltration-front temperature against silicon content in each system on the Mg-Si phase diagram. SiC diameter; ( ■ ): 8 μm, ( ▲ ): 3 μm, ( ▼ ): 2 μm, L: liquid.

apparent that three points marked with asterisks (*) of 15 mass % $SiO_2$ reach the threshold value, and above this $SiO_2$ content, the infiltration-front temperature becomes lower than the liquidus. This means that the amount of $Mg_2Si$ crystallized during infiltration abruptly increases above 15 mass % $SiO_2$, resulting in strong disturbance of the infiltration. Therefore, it is concluded that the major factor influencing the steep drop in infiltration rate is the disturbance caused by the crystallization of $Mg_2Si$ during infiltration. Hence, $SiO_2$ has two opposite effects on the infiltration rate such as an acceleration factor by the increasing infiltration-front temperature and a deceleration factor by the formation of MgO and $Mg_2Si$.

## 7.4 Conclusions

The magnesium composite was fabricated by applying a spontaneous infiltration phenomenon. The main results are as follows.

(1) The spontaneous infiltration of the [SiC + $SiO_2$] powder blend with the magnesium melt occurred under an argon atmosphere at 973 K. $SiO_2$ content necessary for spontaneous infiltration depends on the SiC diameter.

(2) The spontaneous infiltration occurs by improving wettability between the magnesium melt and the SiC particle by elevating the infiltration-front temperature through the Mg-$SiO_2$ thermit reaction.

(3) The factors accelerating the infiltration velocity are the increasing infiltration-front temperature due to Mg-$SiO_2$ thermit reaction and the increasing hydraulic radius due to increasing SiC diameter. On the contrary, the factors decelerating the infiltration velocity are the two reaction products of MgO and $Mg_2Si$.

## References

1) H. Kaneda and T. Choh: J. Mater. Sci., 32 (1997), 47.

2) S-Y. Oh, J. A. Cornie and K. C. Russell: Proc. Ceram. Eng. Sci., 8 (1987), 912.

## 8. Synthesis of $Al_2O_3$ Matrix Composites by Reactive Infiltration

### 8.1 Introduction

In this work, nickel oxide (NiO) and aluminum were used as the starting materials, and the spontaneous infiltration of NiO-base powder blend with molten aluminum was attempted[1]. The reaction between aluminum and NiO is given by: $3NiO + 2Al \rightarrow Al_2O_3 + 3Ni$. In reactive synthesis, it should be noted that a sharp increase in the temperature due to the exothermic nature of the reaction is expected. In order to absorb the heat of reaction and thus control the increase in the temperature caused by the exothermic reaction, $TiB_2$ particles were blended with the NiO powder, because $TiB_2$ is a stable in molten aluminum.

### 8.2 Experimental Procedure

The starting materials are NiO particles (99 %, 44~105 μm), $TiB_2$ particles (99.5 %, under 44 μm) and an aluminum ingot (99.99 %). The $TiB_2$ particles were blended with the NiO particles. The aluminum ingot (8.0 g) was placed on the loose [NiO + $TiB_2$] powder blend (3.0 g), that was located in the bottom of the $Al_2O_3$ crucible. The specimen was heated up to 1673 K in a nitrogen atmosphere, and held for 3600 s. After cooling, the specimen was sectioned and examined by SEM, EPMA and XRD. The differential thermal analysis (DTA) was performed for the consolidated powder blend with the mole ratio of 3:2 (NiO:Al).

### 8.3 Results and discussion

#### 8.3.1 *Effect of $TiB_2$ blending on the infiltration kinetics and the structure of the composite*

It was confirmed by XRD analysis that X-ray peaks of $Al_2O_3$ are detected, whereas those of NiO were rarely detected, suggesting the complete conversion of the NiO particles to $Al_2O_3$ by the given processing condition. The nickel produced immediately reacts with the aluminum to produce $Al_3Ni$. A few peaks of aluminum are also observed, indicating the presence of a minute quantity of aluminum in the composite.

The infiltrated ratio (infiltrated depth / total depth of the powder blend) is shown in Fig. 8-1 as a function of the $TiB_2$ content in the [NiO + $TiB_2$] powder blend. The infiltration barely occurred at $TiB_2$ contents in the range of 0–15 vol %. However, the complete infiltration was achieved when the $TiB_2$ content was greater than a threshold value (15~20 vol %).

Vertical cross-sections of the infiltrated region were observed by SEM for specimens with 5 and 25 vol % of $TiB_2$ particles (Fig. 8-2 (a) and (b), respectively). A continuous film of $Al_2O_3$ is clearly identified in Fig. 8-2(a). This continuous nearly-monolithic $Al_2O_3$ is produced through a melting-solidification process, and thus it infers that the increase in the temperature caused by the exothermic reaction exceeded the melting point of $Al_2O_3$. Unlike the microstructure shown in Fig. 8-2(a), the $Al_2O_3$ formed *in situ* did not have the form of a continuous film at 25 vol % $TiB_2$ (Fig. 8-2(b)). The $TiB_2$ particles were embedded in the $Al_2O_3$ matrix, and $Al_3Ni$ was observed to form at gaps between the $TiB_2$ and $Al_2O_3$. According to the Al-Ni phase diagram[2], the decomposition temperature of $Al_3Ni$ is 1127 K, whereas the processing temperature employed here is 1673 K. Hence, $Al_3Ni$ was a liquid during the holding process and the gaps between the $TiB_2$ particles and the *in situ*-formed$Al_2O_3$ could be the infiltration pathway. Since the $TiB_2$ particles acts as a heat absorber of the heat of reaction, the temperature of the system decreases with an increase in the $TiB_2$ con-

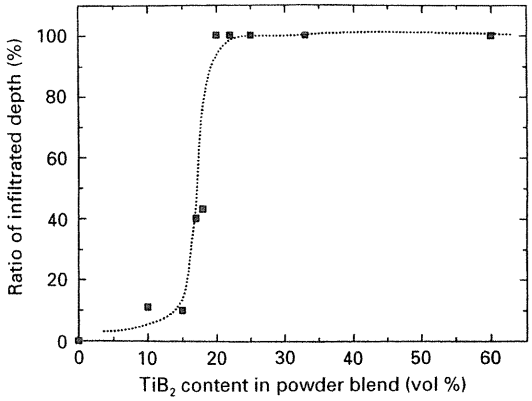


Fig. 8-1 Ratio of the infiltrated depth as a function of the $TiB_2$ content in the powder blend.

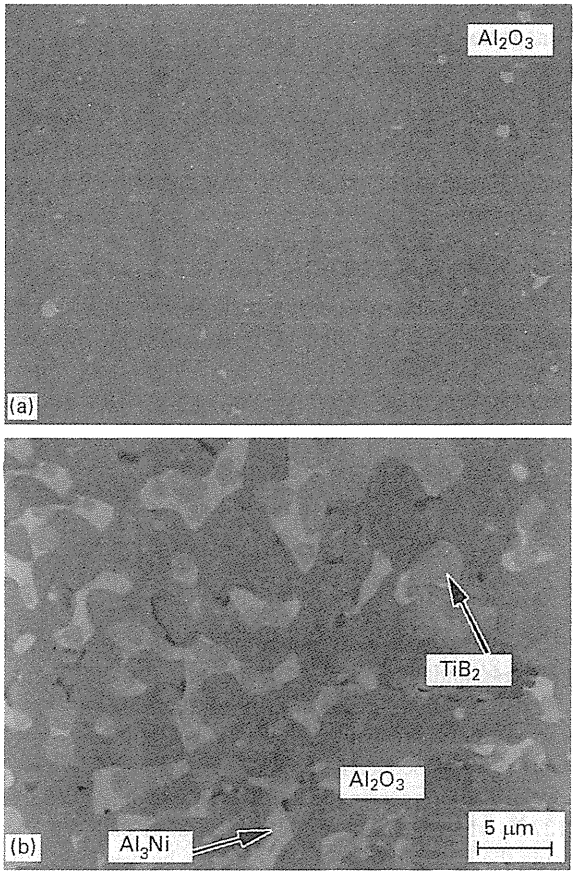


Fig. 8-2 Scanning electron micrographs for specimens with (a) 5 vol % and (b) 25 vol % $TiB_2$ in the powder blend.

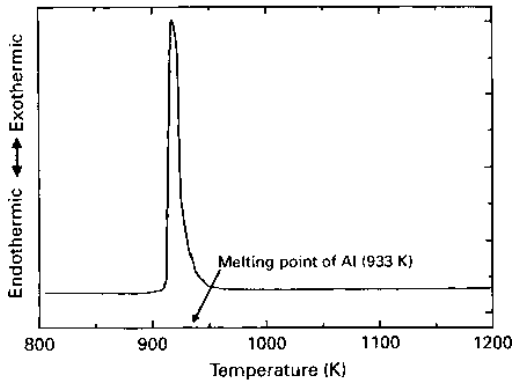


Fig. 8-3 Differential thermal analysis curve obtained from the [NiO + Al] powder compact. The mixture has a mole ratio of Al:Ni of 2:3.

tent. Consequently, the formation of molten $Al_2O_3$ could be prevented by adding more than 20 vol % of $TiB_2$ in the powder blend. From these observations, it can be concluded that the addition of $TiB_2$ (i) decreases the temperature of the system, which prevents $Al_2O_3$ from melting and forming a continuous phase and (ii) helps produce the rout for the infiltration.

### 8.3.2 *Differential thermal analysis (DTA) and adiabatic temperature*

DTA was conducted to identify the initiation temperature of the *in situ* reaction. The DTA profile shown in Fig. 8-3 revealed one sharp exothermic peak at around 930 K, which is near the melting point of aluminum. No endothermic peak indicating the fusion of aluminum was detected. The reaction between NiO and aluminum, therefore, occurs on the melting of the aluminum. From the DTA result, it is apparent that the *in situ* reaction takes place when molten aluminum and NiO come into contact at the infiltration front.

According to the results above mentioned, the system changes through the reaction as follows; before infiltration: [3NiO + 11Al + $x$TiB$_2$] and after infiltration: [$Al_2O_3$3 + 3$Al_3$Ni + $x$TiB$_2$], where $x$ denotes the amount of $TiB_2$ added to the powder phase. The adiabatic temperature ($T_1$), of this reaction can be calculated by the following equation.

$$\Delta H_{f,Al_2O_3} + \int_{T_0}^{T_{m,Al_2O_3}} C_{P,Al_2O_3}dT + 3\int_{T_0}^{T_{m,Al_2O_3}} \left(C_{P,Ni} + C_{P,Al}\right) dT + x\int_{T_0}^{T_{m,Al_2O_3}} C_{P,TiB_2}dT$$

$$+ V_m\Delta H_{m,Al_2O_3} + \int_{T_{m,Al_2O_3}}^{T_1} C_{P,Al_2O_3}dT + 3\int_{T_{m,Al_2O_3}}^{T_1} \left(C_{P,Ni} + C_{P,Al}\right)dT + x\int_{T_m}^{T_1} C_{P,TiB_2}dT = 0$$

where $\Delta H_f$ is the heat of formation, $T_m$ is the melting point, $V_m$ is the mole fraction of molten $Al_2O_3$, $C_p$ is the heat capacity and $\Delta H_m$ is a latent heat of fusion. An initial temperature ($T_0$) of 933 K (the melting point of aluminum) was used in the calculation. Then, the adiabatic temperature was calculated as a function of $TiB_2$ content (Fig. 8-4). The adiabatic temperature shows a constant decrease with increasing the $TiB_2$ content until it reaches a plateau at the melting point of $Al_2O_3$. The transfer of $Al_2O_3$ from a liquid phase to a solid phase was calculated to begin at 25 vol % $TiB_2$. The minimum $TiB_2$ content to induce the spontaneous infiltration was then estimated to be

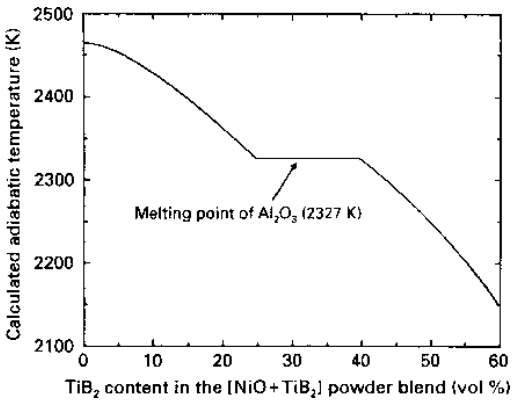


Fig. 8-4 Calculated adiabatic temperature of the system as a function of the $TiB_2$ content in the [NiO + Al] powder blend.

in the range of 25–40 vol %, although the practical minimum $TiB_2$ content required for the infiltration was 15–20 vol %. Therefore, the assumption of the adiabatic system may not be valid in practice and the dissipation of heat should be taken into account. Nevertheless, this calculation does reproduce the fundamental trend of the shift from non-infiltration to fully-infiltrated with an increase in the $TiB_2$ content.

## 8.4 Conclusions

Spontaneous infiltration of the [NiO + $TiB_2$] powder blend with molten aluminum to obtain $Al_2O_3$ matrix composites was attempted at 1673 K. The results obtained in this experiment were:

(1) The addition of $TiB_2$ particles assisted the spontaneous infiltration when the content of $TiB_2$ particles in the [NiO + $TiB_2$] powder blend was more than 20 vol %, whereas the infiltration hardly occurred at $TiB_2$ contents less than 15 vol %.

(2) The specimens mainly consisted of continuous $Al_2O_3$, $TiB_2$ particles and $Al_3Ni$ after the in situ reaction. Gaps between the $TiB_2$ and $Al_2O_3$ were filled by the $Al_3Ni$.

(3) The reaction between NiO and aluminum is initiated at the melting point of the aluminum

## References

1) M. Kobashi and T. Choh: J. Mater. Sci., 32 (1997), 6279.
2) M. F. Singleton, J. L. Murray and P. Nash, in “Binary Alloy Phase Diagrams,” Vol.1, edited by T. B. Massalaski (ASM International, Materials Park OH, 1990) p. 183.

**Acknowledgments**

The author would like to express his sincere gratitude to Dr. M. Kobashi as the Research Associate and Dr. H. Nakata, Dr. H. Kaneda and Dr. E. Taheri-Nassaj as the graduate student for the accomplishment of this study. This work was partly supported by a Ministry of Education (Japan) Grant-in-Aid for scientific research (B). The author is also indebted to his colleagues and many students for their helpful collaboration.